AFRL-SR-BL-TR-98-

0644

REPORT DOCUMENTATION PAGE

1. AGENCY USE ONLY *(Leave blank)*	2. REPORT DATE	3. REPORT TYPE AND DATES COVERED
		Final 01 Aug 96 to 31 Jul 98

4. TITLE AND SUBTITLE
(DURIP 96) High Resolution Diagnostics for Plasma in High Power Microwave Sources

5. FUNDING NUMBERS
61103D
3484/US

6. AUTHOR(S)
ProfessorGilgenbach

7. PERFORMING ORGANIZATION NAME(S) AND ADDRESS(ES)
University of Michigan
3003 South State Street
Wolvering Tower Rm1058
Ann Arbor MI 48109-1274

8. PERFORMING ORGANIZATION REPORT NUMBER

9. SPONSORING/MONITORING AGENCY NAME(S) AND ADDRESS(ES)
AFOSR/NE
110 Duncan Avenue RmB115
Bolling AFB DC 20332-8050

10. SPONSORING/MONITORING AGENCY REPORT NUMBER
F49620-96-1-0374

11. SUPPLEMENTARY NOTES

12a. DISTRIBUTION AVAILABILITY STATEMENT
APPROVAL FOR PUBLIC RELEASED; DISTRIBUTION UNLIMITED

12b. DISTRIBUTION CODE

13. ABSTRACT *(Maximum 200 words)*

The gyrotron microwave source is driven by the Michigan Electron Long Beam Accelerator (MELBA) which operates at -0.8, 1-10 kA, and 0.5-1.5uS pulselength. The correlation was measured between optical spectroscopic emission versus microwave power and pulselength. It was forund that the optical emission from hydrogen H-a radiation was correlated with microwave power and inversely related to microwave pulselength. The physical mechanism is related to plasma accreted from water vapor on the inside of the microwave cavity and collector. This water is ablated and dissociated to release hydrogen. This microwave network analyzer was utilized to obtain cold tests of microwave structures in a rectangular-cross-section gyrotron and a coaxial gyrotron. The primary cold-cavity modes were measured and agreed very well with the results of heterodyned high power microwave signals analyzed by time-frequency analysis. Frequency chirping and mode hopping due to voltage fluctuations were observed as other possible causes of pulse shortering.

14. SUBJECT TERMS

15. NUMBER OF PAGES

16. PRICE CODE

17. SECURITY CLASSIFICATION OF REPORT	18. SECURITY CLASSIFICATION OF THIS PAGE	19. SECURITY CLASSIFICATION OF ABSTRACT	20. LIMITATION OF ABSTRACT
UNCLASSIIFIED	UNCLASSIFIED	UNCLASSIFIED	UL

Final Report to:
The Air Force Office of Scientific Research
on the DURIP Project:

"High Resolution Plasma Diagnostics for High Power Microwave Studies"

Grant Number: F49620-96-1-0374

Submitted by:
Ronald M. Gilgenbach
Professor and Lab Director
Nuclear Engineering and Radiological
Sciences Department
University of Michigan
Ann Arbor, MI 48109-2104

September 1998

Table of Contents page

Executive Summary

This final report documents a research program to discover the cause of microwave pulse shortening by high resolution plasma diagnostic equipment. The following high resolution equipment was purchased:
1) Optical spectrometer system ($60,525)
2) Microwave Network analyzer ($70,409)
These were combined with a high resolution frequency counter (purchased with $12,237 in University of Michigan cost sharing).

The gyrotron microwave source is driven by the Michigan Electron Long Beam Accelerator (MELBA) which operates at -0.8 MV, 1-10 kA, and 0.5-1.5 μs pulselength. The correlation was measured between optical spectroscopic emission versus microwave power and pulselength. It was found that the optical emission from hydrogen H-α radiation was correlated with microwave power and inversely related to microwave pulselength. The physical mechanism is related to plasma accreted from water vapor on the inside of the microwave cavity and collector. This water is ablated and dissociated to release hydrogen. (A continuing AFOSR/MURI program is exploring techniques to remove water from surfaces by RF plasma processing.)

The microwave network analyzer was utilized to obtain cold tests of microwave structures in a rectangular-cross-section gyrotron and a coaxial gyrotron. The primary cold-cavity modes were measured and agreed very well with the results of heterodyned high power microwave signals analyzed by time-frequency analysis. Frequency chirping and mode hopping due to voltage fluctuations were observed as other possible causes of pulse shortening.

1.0 Equipment Purchased

High Resolution Optical Spectroscopy System

from Princeton Instruments, Inc.,

at $60,525 includes:

Acton Research Spectra-Pro750 Spectrograph (0.75 m) with

Accessories = $22,540, includes:

Dual entrance port option

Motorized order sorting filter wheel assembly

Ruled grating, 150g/mm, 500 nm blaze wavelength

Ruled Grating, 1200 g/mm, 500 nm blaze wavelength

Ruled grating 3600 g/mm, 500 nm blaze wavelength

Universal photomultiplier tube housing

Photomultiplier tube

High voltage power supply for PM tube

Spectracard data acquisition card

Intensified, fiber-optic coupled CCD System= $37,985, includes:

Intensified, fiber-optic coupled CCD camera -ICCD-576MG/RB:

High Speed serial Interface controller, ST-138S

Programmable gate pulse generator, PG-200

Real time data acquisition, graphics display, and data processing,

CSMA and Winspec software

*All prices reflect discounts to University of Michigan

High Resolution Microwave Measurement System

from Hewlett Packard, price* = $70,409,

includes:

Network Analyzer-HP8722C, from 50 MHz to 40 GHz,

Option 001: 1 Hz resolution

Option 802: Dual disk drive

Option 913: Rack mount kit

Equipment Purchased by University of Michigan Cost Sharing:

Pulse/ CW Microwave Counter,

from Hewlett-Packard,

price* = $12,237

includes:

Pulse/CW Frequency Counter-HP 5361B

Option 006: Microwave limiter

Option 908: Rack mount

Option 910: Additional Operating and Programming Manual

*All prices reflect discounts to University of Michigan

2.0 Experimental Research

The AFOSR/MURI program experimental configuration of DURIP equipment is depicted in the overview of Figure 1 and the detailed schematic of Figure 2. The gyrotron electron beam is driven by explosive emission from the MELBA cathode stalk (-0.8 MV, 1-10 kA, 0.5-1 μs). The electron beam propagates through a magnetic cusp to generate a rotating, axis encircling electron beam. Most earlier experiments were performed with a rectangular cross section gyrotron, as shown in Fig. 1. Later experiments utilized the new coaxial gyrotron, which is still under AFOSR/MURI investigation (Fig. 3).

The fiberoptic probe was initially pointed down the axis of the microwave tube as shown in Fig. 1; this caused the spectroscopic equipment to measure Al emission from the e-beam diode. Later experiments used individual optical fibers which were located to view specific regions of the tube, such as cavity or collector (Fig. 3).

The spectrally-resolved hydrogen H-alpha line is shown in Figure 4. Two small carbon peaks are also visible. The magnitude of the strongest emission, from this H-α peak, was utilized to diagnose the plasma in the microwave tube. Residual gas analyzer measurements showed that prior to the shot, water vapor was the dominant impurity. After the shot the concentration of hydrogen dominated, indicating that the e-beam or microwaves dissociated the water vapor.

Experimental results from the rectangular cross-section gyrotron are depicted in Figure 5. The normalized H-α optical

emission correlates quite well with the microwave power for this set of MELBA shots. Figure 6 displays the microwave pulselength and the optical emission counts from the H-α optical emission; a mild anticorrelation exists between these signals.

Time resolved signals of H-α were obtained from a photomultiplier tube, as shown in Fig. 7 for the rectangular cross-section gyrotron and Fig. 8 for the coaxial gyrotron. These data showed that as the microwave signal decreased following a peak, the H-α optical emission gradually increased on a time scale of some 500 ns.

The previous data are consistent with a physical explanation as follows. The electron beam scraping and dumping on the collector liberates water vapor from the walls and dissociates it, releasing hydrogen atoms. The hydrogen travels (at speeds of 1-10 cm/μs) into the output waveguide where it can be broken down by the high power microwaves. The estimated density of the plasma easily exceeds the cutoff density for the 2-4 GHz microwave emission. These results are described in more detail in the attached reprint of the article, which was published in the IEEE Transactions on Plasma Science: "Optical Spectroscopy of Plasma in High Power Microwave Pulse Shortening Experiments Driven by a μs e-Beam".

Results of microwave cold-tests utilizing the Hewlett-Packard network analyzer are shown in Figure 9. These data permitted identification of specific cavity mode frequencies, including: TE_{101}, TE_{011}, TE_{111}, and either TE_{014} or TE_{201} mode. High power rectangular-cross-section gyrotron data are summarized in

Figure 10. It can be seen that the cold test modes frequencies were measured in the high power microwave emission. The previous data were analyzed utilizing a fast-Fourier-transform. We have since discovered that time-frequency-analysis permits high resolution measurements of frequency versus time to observe actual mode hopping between two competing modes, as depicted in Figure 11.

3.0 Publications Resulting from this Research

1) Jonathan Hochman, Doctoral Dissertation: "Microwave Emission of Large and Small Orbit Gyrotron Devices", May, 1998

2) "Time-Frequency Analysis of modulation of high power microwaves by electron-beam voltage fluctuations", C. W. Peters, R.L. Jaynes, Y.Y. Lau, R.M. Gilgenbach, W.J. Williams, J.M. Hochman, W.E. Cohen, J.I. Rintamaki, D.E. Vollers, J. Luginsland and T.A. Spencer, Phys. Rev. E, (November 1998)

3) "Optical Spectroscopy of Plasma in High Power Microwave Pulse Shortening Experiments Driven by a μs e-Beam", R.M. Gilgenbach, J.M. Hochman, R.L. Jaynes, W.E.Cohen, J.I. Rintamaki, C.W. Peters, D.E.Vollers, Y.Y. Lau, and T.A. Spencer, IEEE Transactions on Plasma Science, Special Issue on High Power Microwaves, 26 282 (1998)

4) "Polarization control of microwave emission from high power rectangular cross section gyrotron devices, J.M. Hochman, R.M. Gilgenbach, R.L. Jaynes, J.I. Rintamaki, Y.Y. Lau, W.E. Cohen, C. Peters,

and T.A. Spencer, IEEE Trans. Plasma Sci., Special Issue on HPM, 26 383 (1998)

4.0 Graduate Student Training

A number of students utilized the equipment funded by DURIP.

1) Jon Hochman, Ph.D., former graduate student, rectangular-cross section gyrotron,

2) Reggie Jaynes, graduate student, coaxial gyrotron,

3) Josh Rintamaki, graduate student, Sandia Project on diode physics,

4) Bill Cohen, graduate student, plasma measurements in gyrotrons,

5) Doyle Vollers, Captain, USAF, graduate student, thermionic cathode (blackbody spectrum),

6) Mark Johnston, summer visiting student, thermionic cathode (blackbody spectrum).

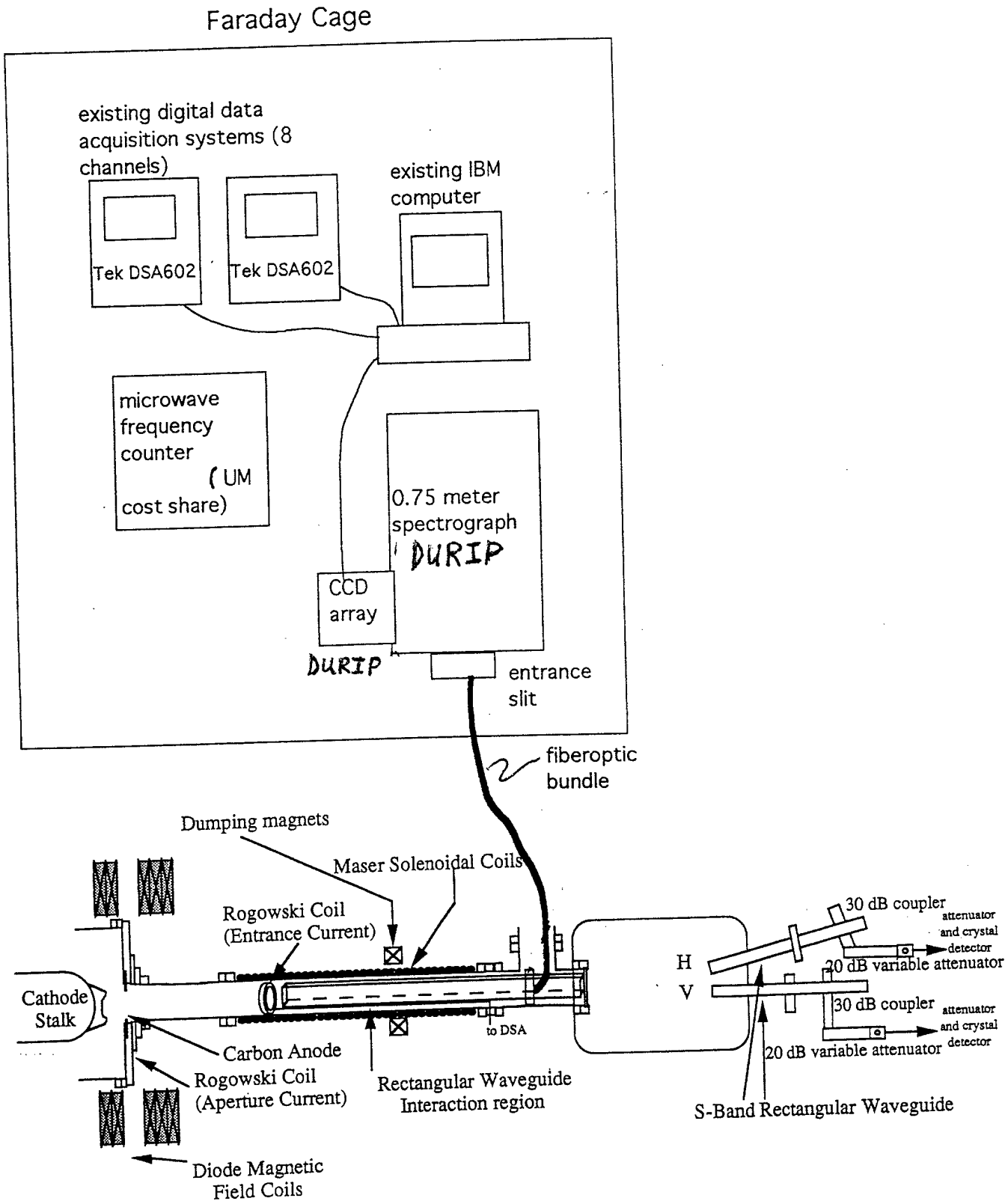

Figure 1. Experimental configuration.

ICCD Spectrograph System Setup

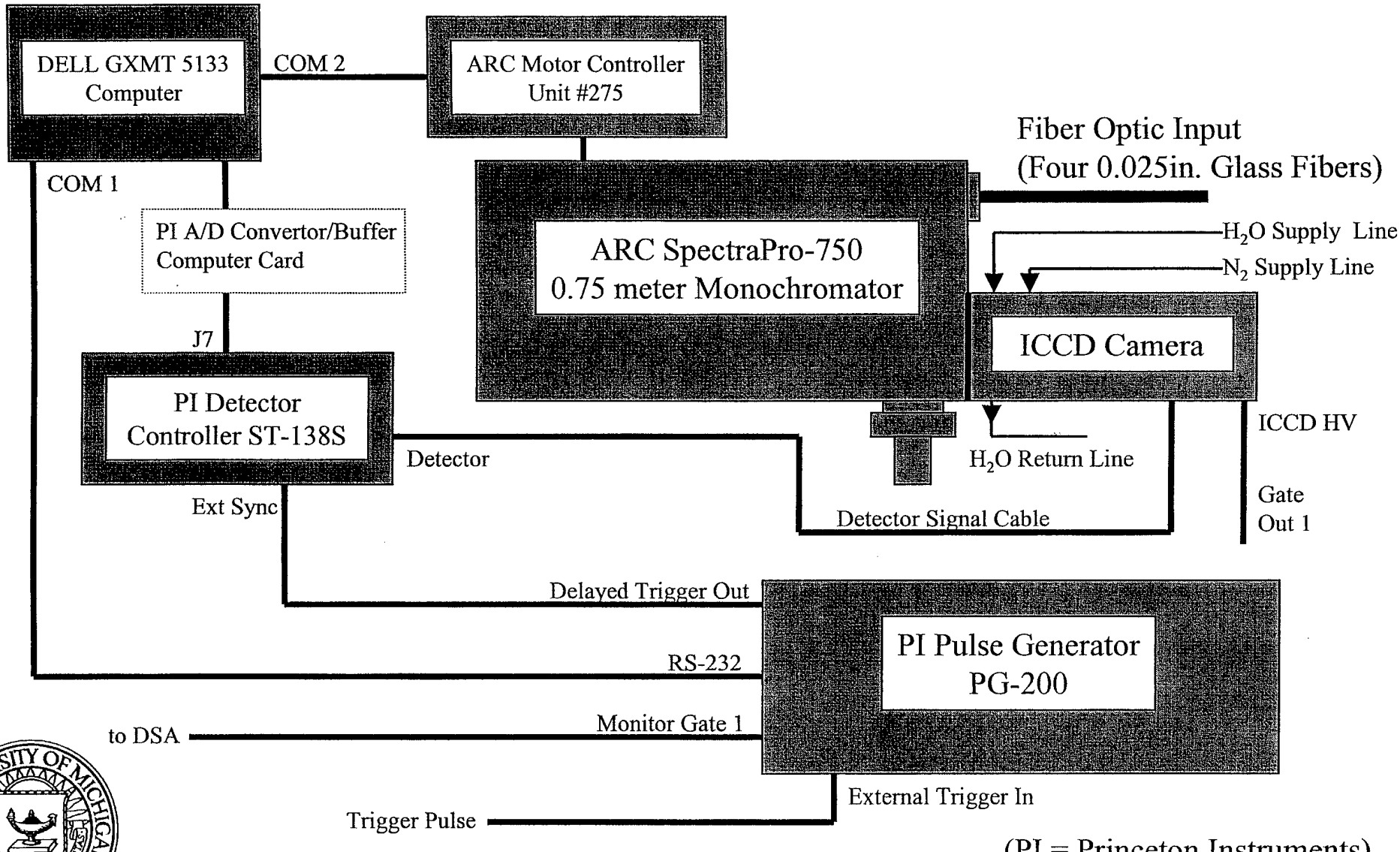

(PI = Princeton Instruments)

Spatially Resolved Fiber Optic Probes

(Fiber Optic Setup #2 - Coaxial Gyrotron)

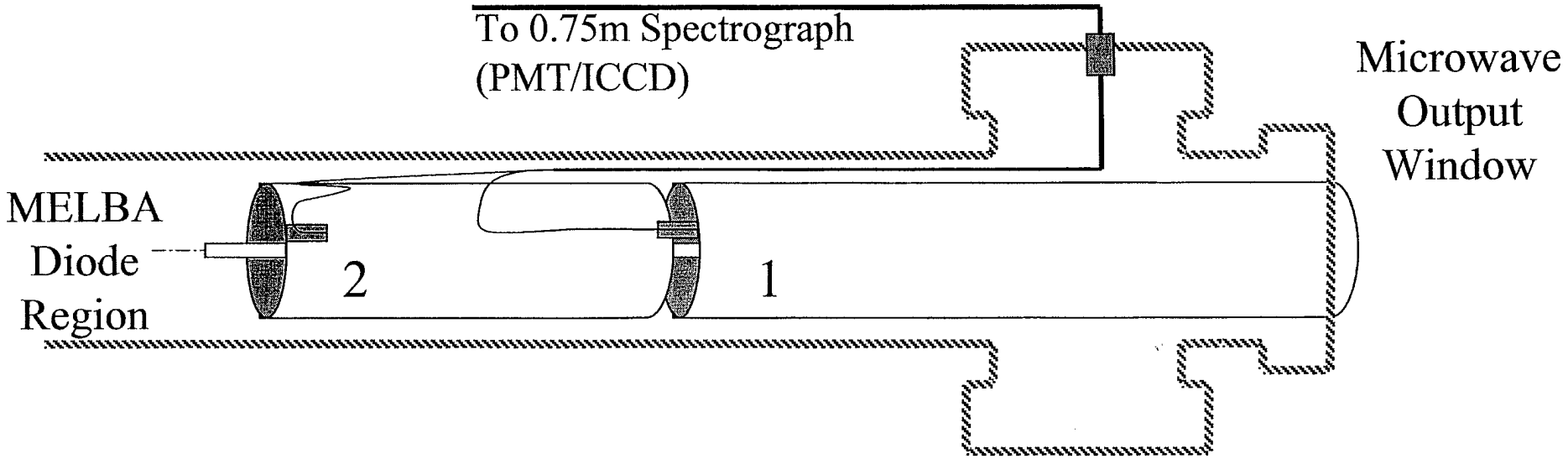

1. Fiber Optic looking along the centerline towards the Microwave Output Window through only the coaxial waveguide region
2. Fiber Optic looking along the centerline towards the Microwave Output Window away from Diode through both the coaxial interaction and waveguide regions

Optical Emission of H-alpha (w/ C II)

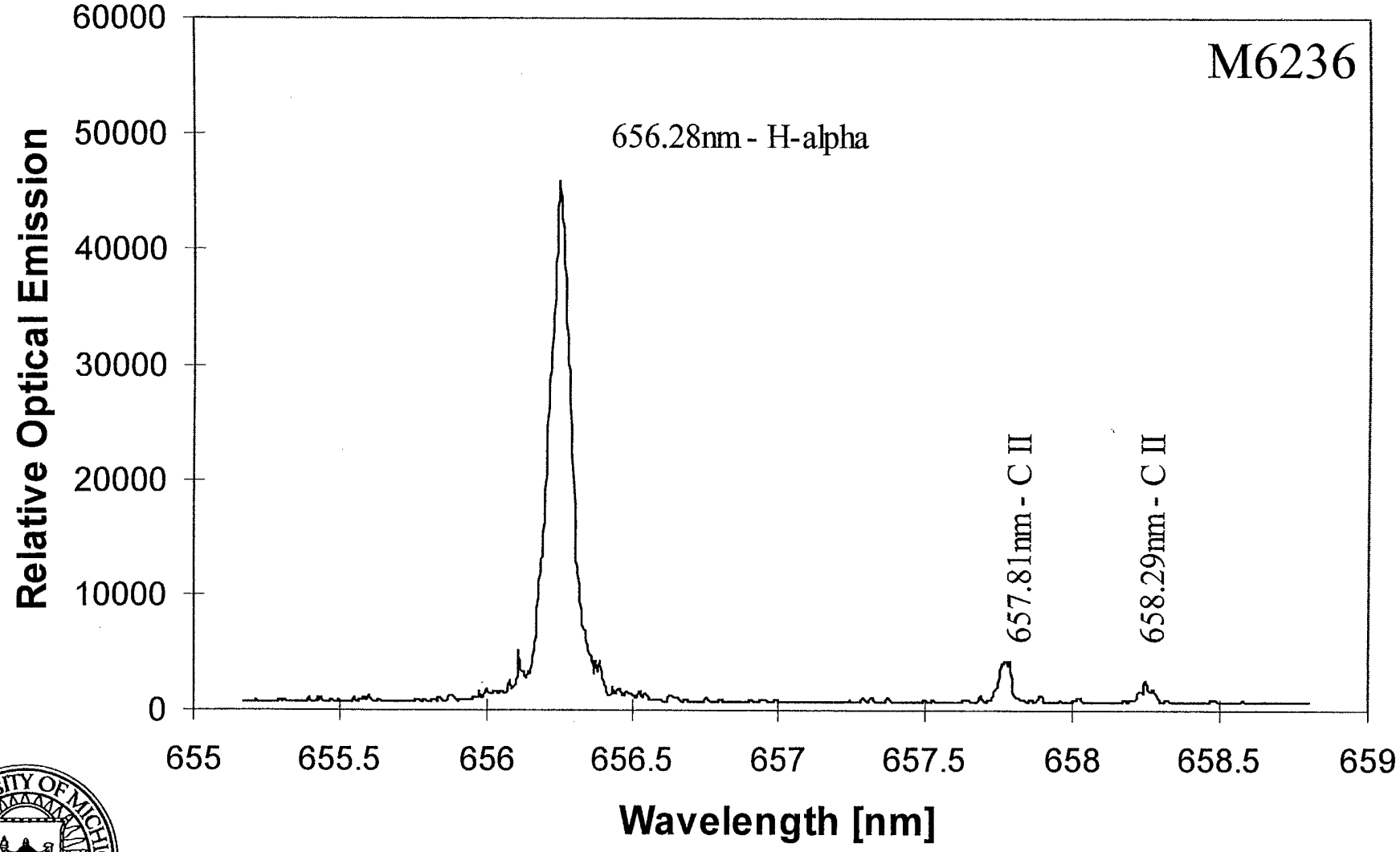

Microwave Power and Optical Emission of H-alpha versus MELBA Shot Number

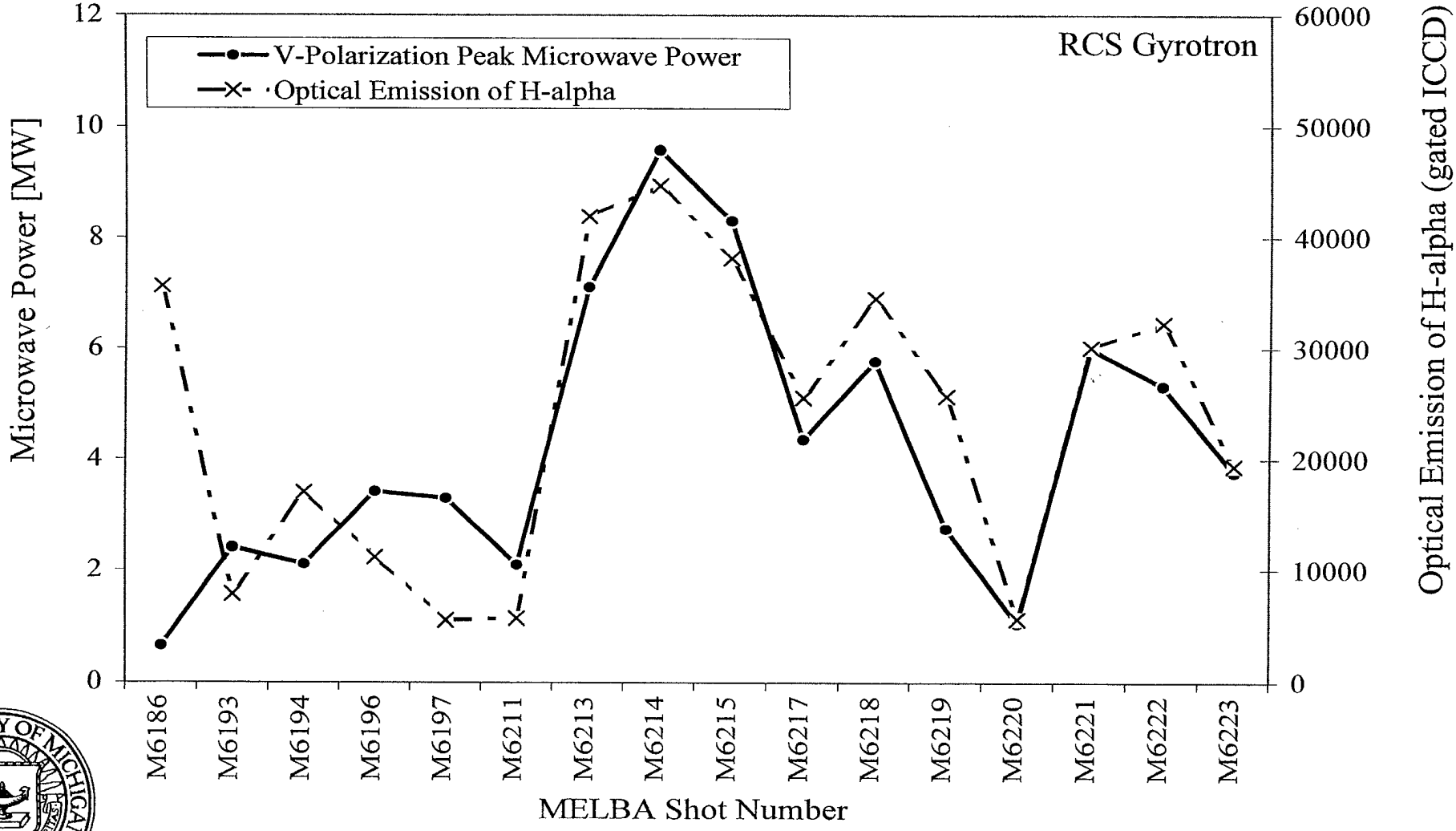

William E. Cohen

Fig. 5

1998 IEEE - ICOPS; Raleigh, North Carolina

Microwave Pulse Length (Vpol) and Optical Emission of H-alpha versus MELBA Shot Number

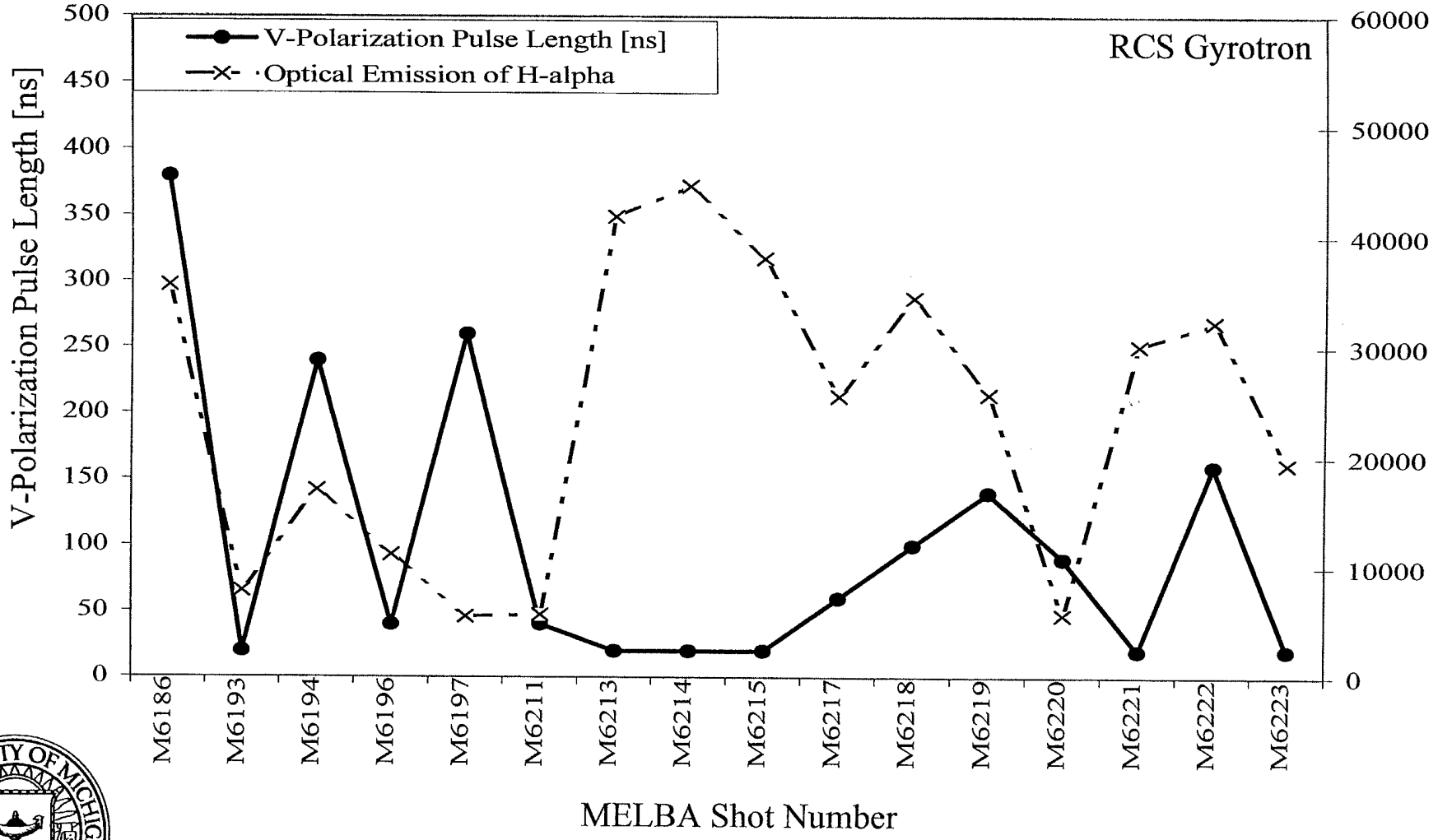

Time Resolved H-alpha Measurement

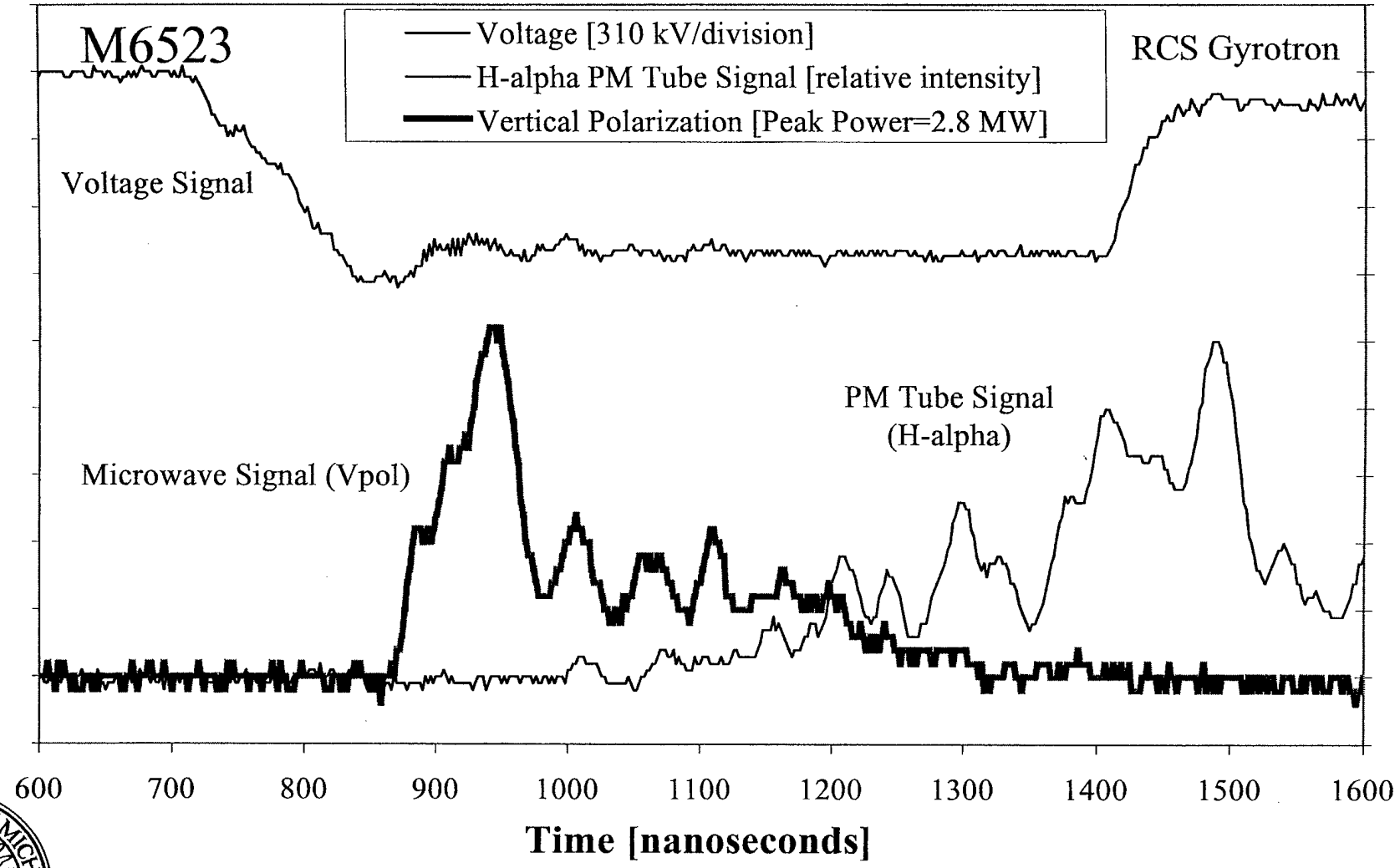

Time Resolved H-alpha Optical Emission

(for Coaxial Interaction and Waveguide Region)

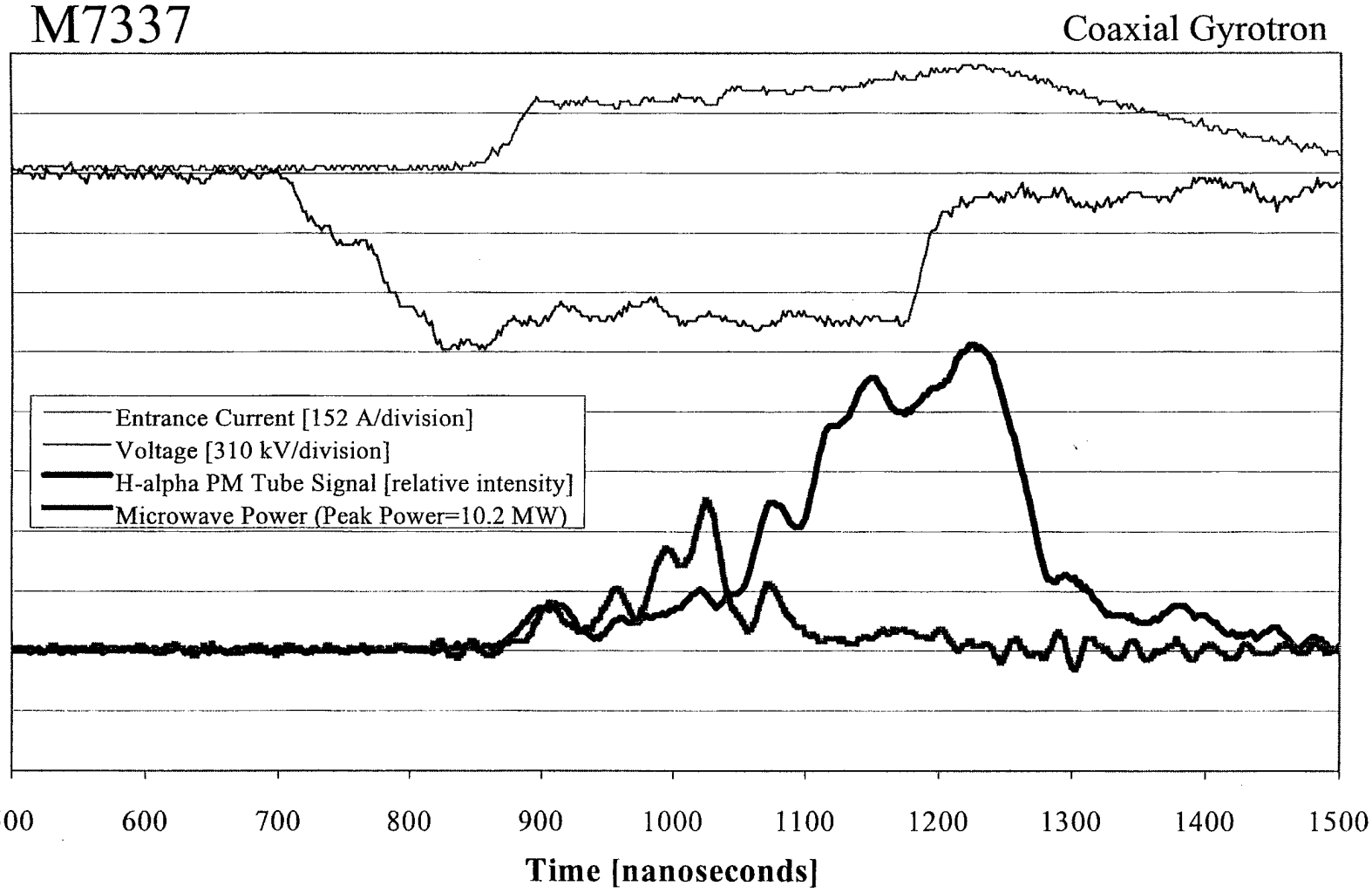

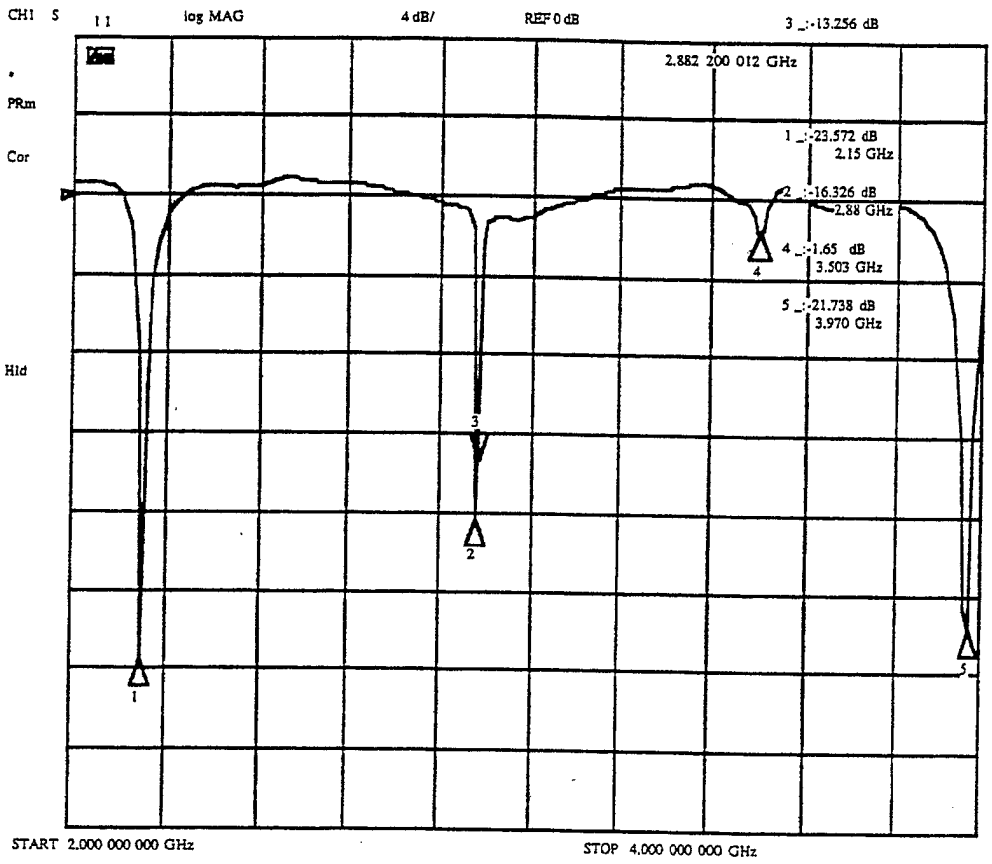

Figure 9. Cold test frequency spectrum of the RCS cavity (cavity A). Marker 1 appears at a frequency of 2.15 GHz. This corresponds to the TE_{101} mode. Marker 2, which appears at 2.88 GHz, corresponds to the TE_{011} mode. Marker 4 shows the TE_{111} mode at 3.50 GHz, and marker 5 is apparently due to either the TE_{014} mode or possibly the TE_{201} mode at 3.97 GHz.

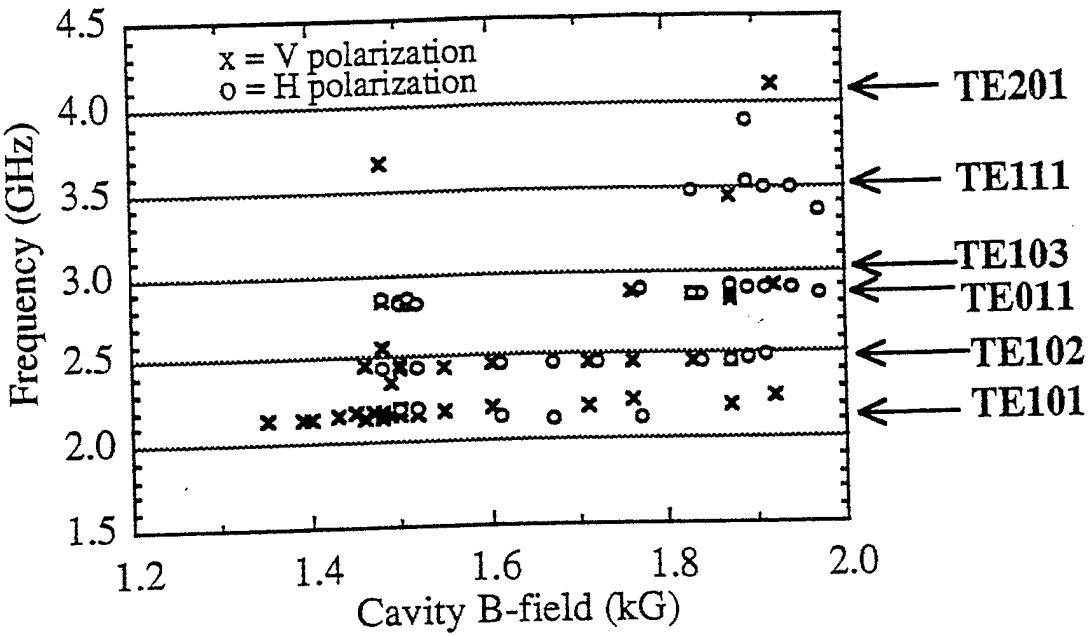

Figure 10 Frequency response of the large orbit gyrotron (cusp II) as a function of cavity B-field. As is clearly evident, mode competition was much worse at higher magnetic fields.

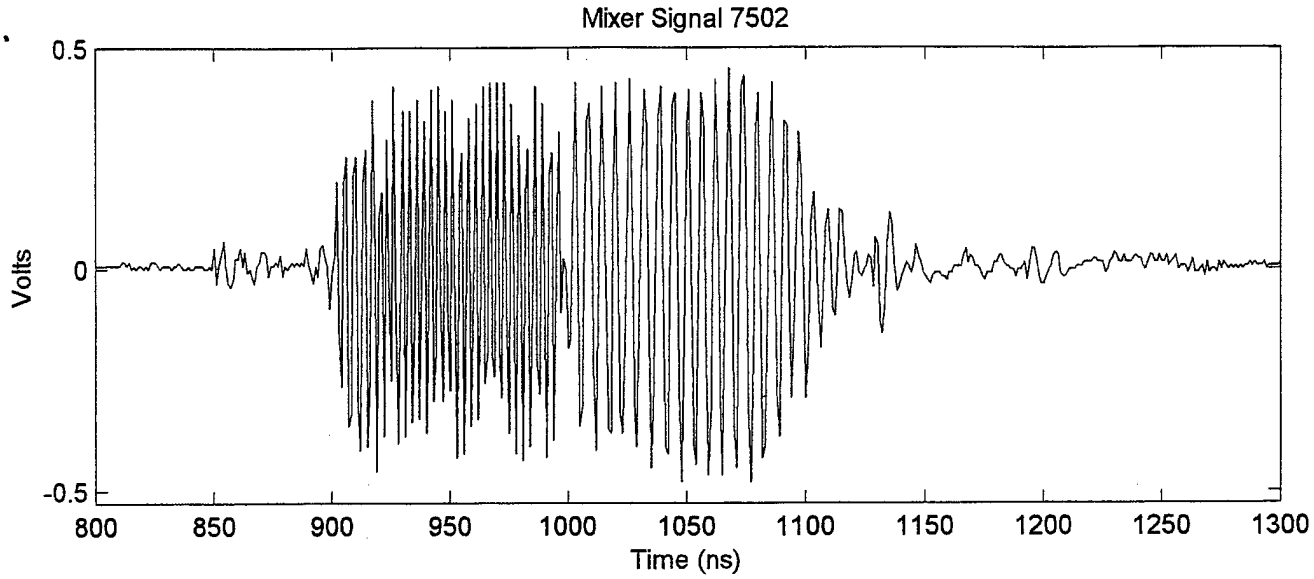
Mixer Signal 7502
0.5
0
-0.5
Volts
800
850
900
950
1000
1050
1100
1150
1200
1250
1300
Time (ns)

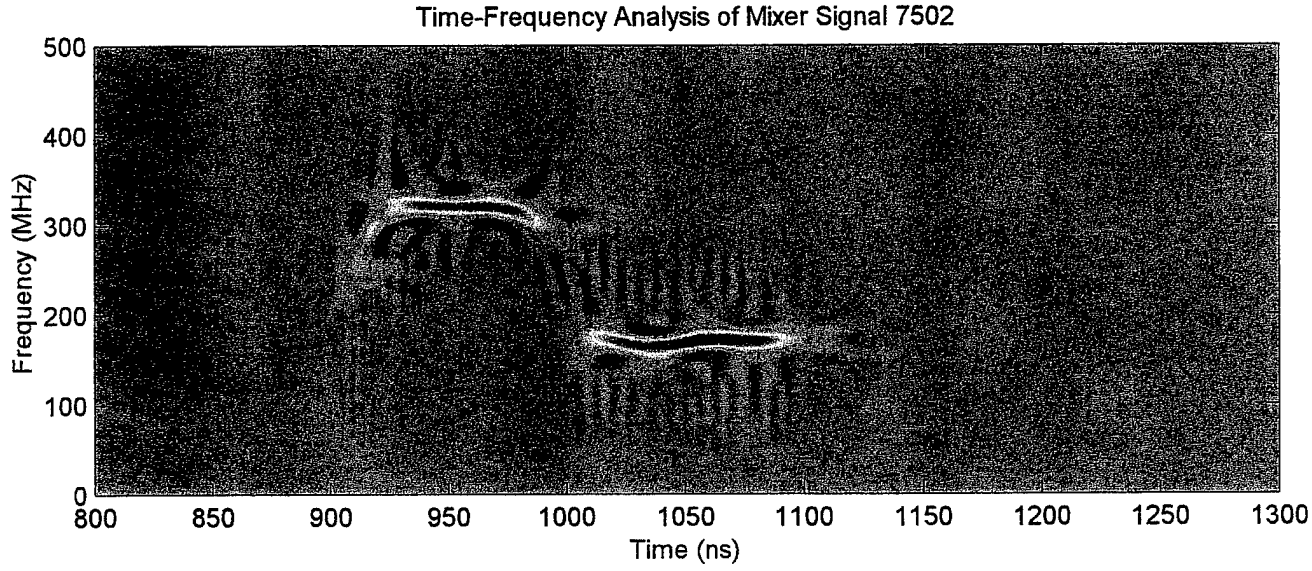
Time-Frequency Analysis of Mixer Signal 7502
500
400
300
200
100
0
Frequency (MHz)
800
850
900
950
1000
1050
1100
1150
1200
1250
1300
Time (ns)

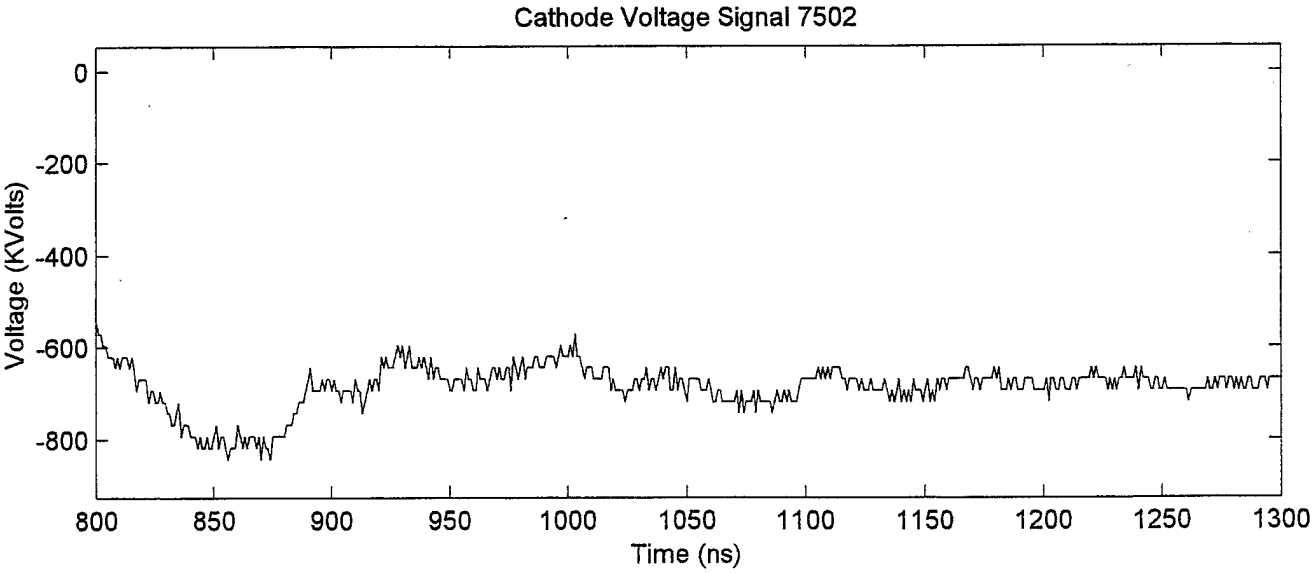
Cathode Voltage Signal 7502
0
-200
-400
-600
-800
Voltage (KVolts)
800
850
900
950
1000
1050
1100
1150
1200
1250
1300
Time (ns)

Fig. 11

Time-Frequency Analysis of Modulation of High Power Microwaves by e-Beam Voltage Fluctuations

C. W. Peters, R. L. Jaynes, Y. Y. Lau, R. M. Gilgenbach, W. J. Williams*,

J. M. Hochman, W. E. Cohen, J. I. Rintamaki, D. E. Vollers, and T. A. Spencer**

Department of Nuclear Engineering and Radiological Sciences

University of Michigan

Ann Arbor, MI 48109-2104

Abstract.

This paper applies a time-frequency analysis to the output signal from a coaxial gyrotron oscillator. It is shown that the voltage fluctuations on the diode can be directly correlated to the frequency modulation on the rf output. A simple analytic theory is constructed to explain this correlation. This technique, properly extended, is expected to open up a new way to investigate pulse shortening, mode competition, noise and unwanted frequencies in rf generation.

*Department of Electrical Engineering and Computer Science, University of Michigan, Ann Arbor, MI 48109

**Air Force Research Laboratory, Kirtland AFB, NM 87117-5776

The most pressing issue in the generation of high power microwaves (HPM) is pulse shortening, that is, the rf output pulse length is significantly less than the duration of the voltage pulse on the diode [1-3]. Depending on the HPM source, variations in the diode conditions due, for example, to an evolving plasma within the diode may lead to departure from the design values. Generation of HPM then ceases. While there are many scenarios being proposed for pulse shortening, most of which are drawn from speculations, few, if any, have been substantiated by a direct correlation between the diode voltage fluctuations and the rf output. Faced with the paucity of such a correlation, we initiated a time-frequency analysis of the output rf from a coaxial gyrotron [4]. The rf modulations were explicitly linked to the diode voltage fluctuations.

As is well-known, from the (time-integrated) spectrum alone, it is virtually impossible to correlate the output signal with diode voltage fluctuations. Recently developed analyses, which permit the display of joint time-frequency spectra, naturally provide such a direct correlation [5-7]. Being essentially a "real-time" diagnostic, this powerful technique can also be applied to study noise, unwanted frequencies, and mode hopping in various rf sources. One simply takes a time-frequency analysis of the output signal, and correlates it with whatever factor (e.g., beam voltage or current fluctution) that is suspected to be the contributing cause, as is done in this work.

To directly show the evolution of the rf in the presence of diode voltage fluctuations, we consider the rf output that is extracted from a coaxial gyrotron. The time-frequency analysis of this output signal shows that the frequency chirp in fact tracks the diode voltage. We provide a simple analytic theory, based on the beam-cyclotron mode, to explain this correlation.

The experimental configuration is depicted in Figure 1. The electron beam is generated by MELBA (Michigan Electron Beam Accelerator [8]) at parameters: energy = 0.75 MeV, I(tube) = 100-300A, and pulselength from 0.5-1 microsecond. Cathode voltage is measured by a resistive divider across the insulating stack. The annular electron beam is generated from plasma flashover on a bare aluminum cathode; nonemitting regions are coated with insulating enamel (Glyptal). This electron beam is extracted through an annular aperture in a graphite anode; anode-cathode gap is 11 cm.

The electron beam is run through a magnetic-cusp field reversal which occurs over 10 cm (- 1.1 kGauss at diode up to +3 kG in the interaction cavity) to generate a large-orbit, axis-encircling electron beam [Fig. 1a]. The e-beam's perpendicular-to-parallel velocity ratio (α) is approximately unity [9]. The gyrotron's inner coaxial rod (6 mm diameter) runs the full tube length from anode to output window. The microwave cavity (outer coaxial tube) has an inside diameter of 7.4 cm and a length of 26 cm. The gyrotron is operated in the TE_{11} coaxial mode. Microwave emission is directed into a large chamber lined with microwave absorber. An open-ended S-band waveguide collects microwave power, which is passed through a directional coupler into coaxial cable. The coaxial cable transmits microwave signal to attenuators and a heterodyne mixer driven by a local oscillator located in a Faraday cage. The intermediate (beat) frequency signal from the mixer is input to a 2 GSa/s digital signal analyzer (Tektronix DSA602); for time synchronization the cathode voltage signal is measured on the same signal analyzer.

The digitally stored intermediate frequency from the mixer is subjected to a time-frequency analysis [5, 6]. Traditionally, joint time-frequency analyses have utilized the spectrogram. The spectrogram is derived from the magnitude-squared Fourier transform of a windowed portion of the signal being analyzed. The spectrogram has been a useful

tool, but it suffers from a time-frequency uncertainty effect because of the analysis window [5]. More recently, joint time-frequency distributions, which avoid the spectrogram windowing effect, have been developed [5]. Reduced interference distributions (RIDs) have been developed over a period of more than ten years at the University of Michigan [6,7]. The Wigner distribution, as known in quantum mechanics [5] provides a methodology for deriving effective joint time-frequency distributions, but suffers from cross-terms or interference terms between time-frequency components. RIDs retain the numerous desirable properties of Wigner distributions, but considerably reduce the troublesome cross-terms [6,7]. Proper representation of group delay and instantaneous frequency along with high resolution time-frequency representation are among the valuable RID properties which are particularly important to this study. The binomial time-frequency distribution [6] is an effective discrete form of RID for computational purposes, and for this reason it was used in the time-frequency analysis presented in this paper. These techniques are particularly effective in the analysis of nonstationary signals and have been applied to biological signals, radar, sonar and other areas. We note that RIDs do not theoretically require windowing to produce their results. Practically, however, finite length data segments much longer than those commonly used in spectrograms are utilized, greatly reducing the time-frequency uncertainty effects observed with spectrograms.

The signal used for analysis is the heterodyne signal. Heterodyne detectors generate a signal in which the frequency is either an upshifted or downshifted beat frequency between the incoming microwave and a local oscillator. The local oscillator is set at the frequency of 2.3 GHz. This frequency corresponds to the cutoff frequency of the TE_{11} mode in the coaxial waveguide, so the microwave frequency equals 2.3 GHz plus the upshifted beat frequency. Figure 2a is the actual output of a heterodyne signal. The time-frequency analysis of this signal is shown in Figure 2b. This figure clearly

shows that there is significant frequency chirp from, for instance, 2.39 GHz (= 2.3 GHz + 90 MHz) at t = 920 ns to 2.51 GHz (= 2.3 GHz + 210 MHz) at t = 960 ns. To correlate this frequency chirp, we display in Fig. 2c the evolution of the diode voltage. A comparison of Figs. 2b and Fig. 2c shows that there is a definite correlation between the frequency modulation and the diode voltage variation -- the microwave frequency lowers when the diode voltage increases (i.e., becomes more negative in Fig. 2c). This direct modulation of the frequency by the diode voltage fluctuations is readily interpreted [See below and Eq. (2)]. We have run many shots and similar correlations are unmistakable. We should add that the time axes in the microwave signals shown in Fig. 2 have taken into account the finite group propagation time that is required for the rf to transport through the output waveguides and the transmission system. Typically, the time-frequency analysis of the heterodyne signal, such as that shown in Figure 2b, shows a shorter interval of HPM generation than the diode voltage pulse. Low level rf signals (not shown) have been detected under certain conditions for almost the entire duration of the voltage pulse, however.

The color intensity shown in Fig. 2b is indicative of the power of the signal (red = higher power, yellow = lower power). By taking the maximum intensity at each time in Fig. 2b, we obtain Fig. 2d which displays the power fluctuations. To verify these power fluctuations, we show in Fig. 2e an independent diode detector measurement of the microwave power generated by the coaxial gyrotron. Both Figs. 2d and 2e show three humps in the microwave power. The differences between these two figures are due to differences in the frequency response of the detectors and filtering in the signal analyzers. Thus, Figs. 2b - 2e strongly suggest this causal sequence of events: fluctuations in the diode voltage lead to fluctuations in the interaction frequencies, which in turn leads to large fluctuations in the output rf power.

The frequency modulation by the diode voltage shown in Fig. 2b and Fig. 2c may be explained as follows. In cyclotron masers, the frequency ω is related to the electron orbit through the beam-cyclotron mode [10]

$$\omega = kv_z + \Omega/\gamma \tag{1}$$

where k is the axial wavenumber, Ω is the nonrelativistic cyclotron frequency of an electron, v_z is the axial velocity of an electron, and γ is the relativistic mass factor. Small variations in the diode voltage, δV, lead to small variations in γ and in v_z, and hence in ω according to Eq. (1). Assuming that the last term in Eq. (1) gives the dominant contribution, we obtain the fractional change in ω in terms of the fractional change in the beam energy (diode voltage):

$$\frac{\delta\omega}{\omega} = -\left(\frac{\delta\gamma}{\gamma}\right)\left(1 - \frac{\gamma}{\beta^2}\frac{kv_z}{\Omega}\right) \approx -0.48\left(\frac{\delta V}{V}\right). \tag{2}$$

In deriving the middle term in Eq. (2), we have used $\beta^2 \equiv v_z^2(1+\alpha^2)/c^2 = 1-\gamma^{-2}$ and assumed that α, the ratio of the perpendicular velocity to the parallel velocity of an electron, is a constant. The numerical value given in the last term of Eq. (2) is obtained by taking a DC magnetic field of 2 kG, $\beta = 0.914$, $\alpha = 1$, corresponding to a diode voltage $V = (\gamma - 1)511$ kV = 750 kV, and $k = \pi/26$ cm = 12 m^{-1}. Note the direct proportionality of diode voltage fluctuations and frequency chirp as shown in Eq. (2) and Figs. (2b) and (2c). The numerical value on the right hand side of Eq. (2) only gives a qualitative indication because (A) there are uncertainties in k and in α, and (B) more importantly, Eq. (2) does not give the frequency dependence in the power distribution in the chirped rf output, so the range of $\delta\omega/\omega$ predicted by Eq. (2) is only an estimate. Using the values of $\delta\omega/\omega$ and $\delta V/V$ inferred from Figs. 2b, 2c, we find that Eq. (2) is satisfied to within 20 per cent.

While this paper provides direct evidence of the consequences of diode voltage fluctuations, namely, frequency chirp and the large fluctuations in the output power in a coaxial gyrotron, it examplifies the tremendous opportunities opened up for a critical examination of pulse shortening, mode competition and interference, noise, and beam loading, etc, most of which are yet to be fully understood. Causal effects can be identified in a real-time analysis, which may also be conveniently adopted in particle simulations. For example, one may apply a time-frequency analysis of the voltages at the various gaps of a relativistic klystron [11] to determine if the loading of the gap(s) by the intense beam, or simply the diode voltage fluctuations as studied in this paper, could lead to pulse shortening. Such an examination may also be applied to computer simulations, and to other high power microwave sources.

This work was supported by the Multidisciplinary University Research Initiative funded by the Air Force Office of Scientific Research through a subcontract to Texas Tech University. It was also supported by DoD/AFOSR/AASERT Grants, and by the Industrial Affiliates Program of the Northrop Grumman Corporation.

References

[1] See, e.g., IEEE Trans. Plasma Sci., Special Issue on High Power Microwave Generation, (June 1998); also, Digest of International Workshop on High Power Microwave Generation and Pulse Shortening, Edinburgh, Scotland, June 10-12, 1997, available at http://library.plk.af.mil/edinburgh/digest.html.

[2] F. J. Agee, "Evolution of pulse shortening research in narrow band, high power microwave sources", in Ref. [1].

[3] D. Price and J. Benford, "General scaling of pulse shortening in explosive-emission driven microwave devices", in Ref. [1].

[4] R. L. Jaynes *et al.*, in IEEE International Conf. on Plasma Science, June 1-4, 1998, Raleigh, North Carolina.

[5] L. Cohen, *Time-Frequency Signal Analysis*, (Prentice Hall, New York, 1995).

[6] W. J. Williams and J. Jeong, in *Time-Frequency Signal Analysis: Methods and Applications*, ed. B. Boashash, (Longman and Cheshire, 1992), Ch. 3, pp. 74 - 98.

[7] W. J. Williams, Proc. IEEE **84**, 1264 (1996).

[8] R. M. Gilgenbach *et al.*, in Proc. 5th IEEE Pulsed Power Conference, June 10-12, 1985, p. 126, [IEEE Catalog Number 85C 2121-2].

[9] J. M. Hochman, "Microwave emission of large and small orbit rectangular gyrotron devices", Doctoral Dissertation, University of Michigan, Ann Arbor, 1998.

[10] See, e.g., V.L. Granatstein and I. Alexeff, eds., *High Power Microwave Sources*, (Artech House, Norwood, 1987).

[11] See, e.g., K. J. Hendricks *et al.*, Phys. Rev. Lett. **76**, 154 (1996), and references therein.

Figure Captions

Fig. 1. Configuration of coaxial, large-orbit gyrotron.

a) typical axial magnetic field profile as a function of axial distance z,

b) experimental schematic drawing.

Fig. 2. Analysis of output microwaves from coaxial gyrotron.

a) heterodyne detector signal with local oscillator set at 2.3 GHz,

b) joint time-frequency spectra from reduced interference distributions (RID) analysis: red is higher power, yellow is lower power,

c) cathode voltage signal,

d) intensity from RID program,

e) microwave diode detector signal; peak corresponds to 1.2 MW; smoothed by a 20 MHz lowpass filter.

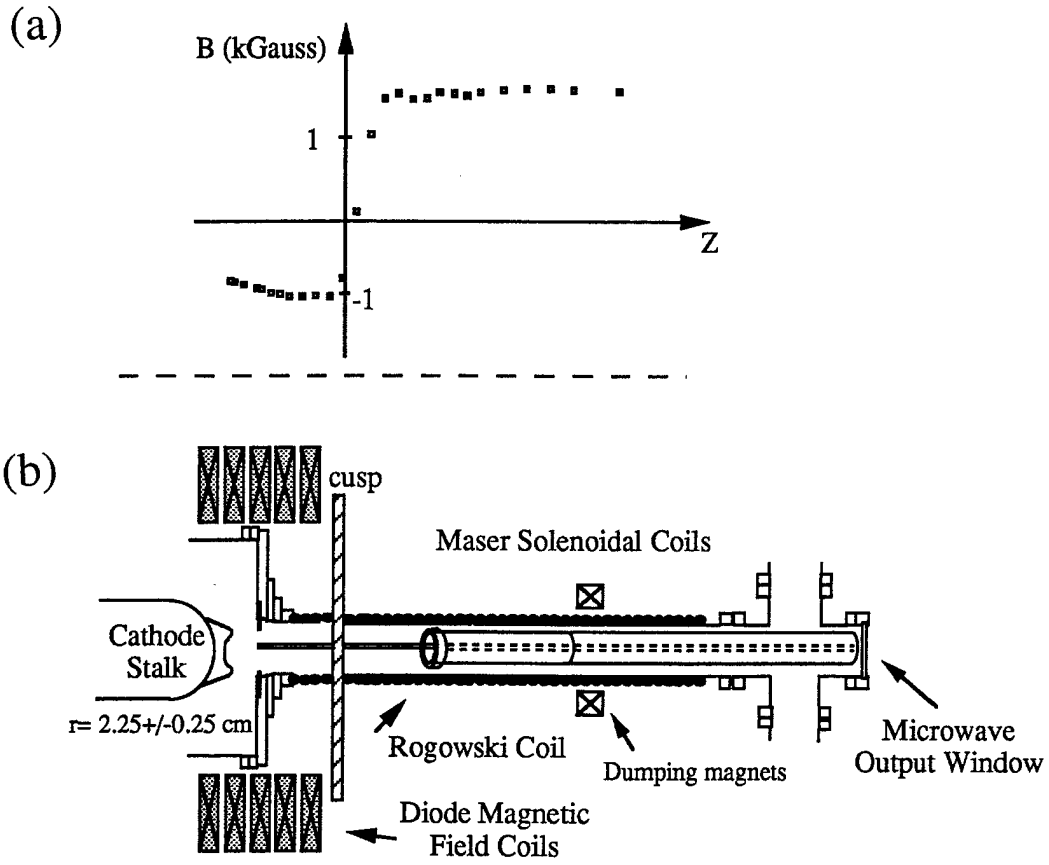
(a)
B (kGauss)
1
-1
z
(b)
cusp
Maser Solenoidal Coils
Cathode
Stalk
r= 2.25+/-0.25 cm
Rogowski Coil
Dumping magnets
Microwave
Output Window
Diode Magnetic
Field Coils

Fig. 1

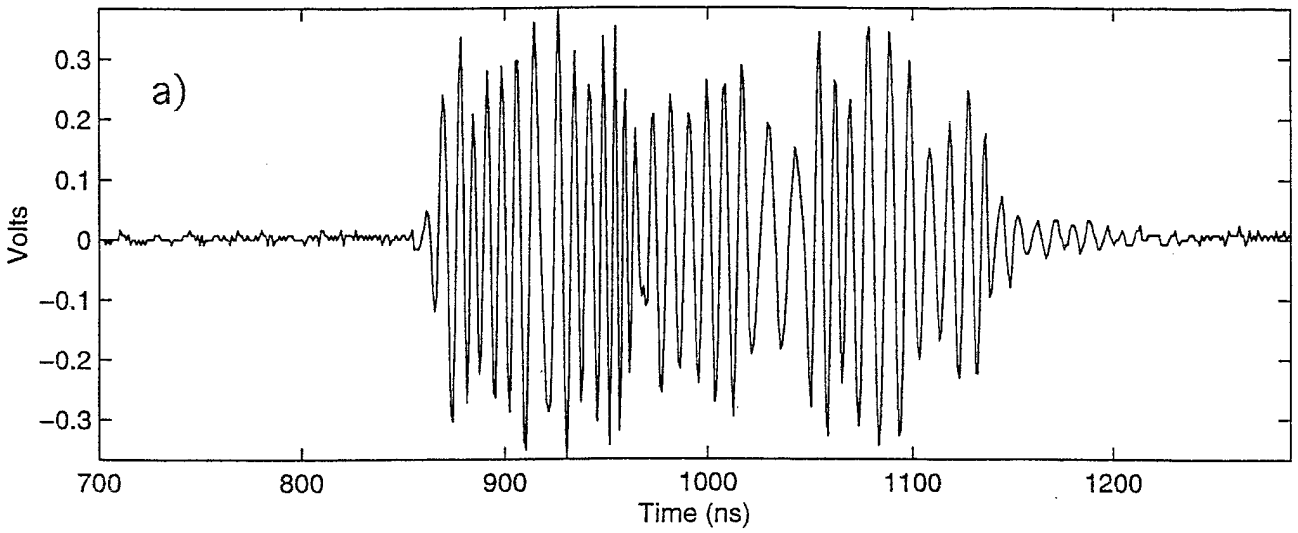

Fig. 2

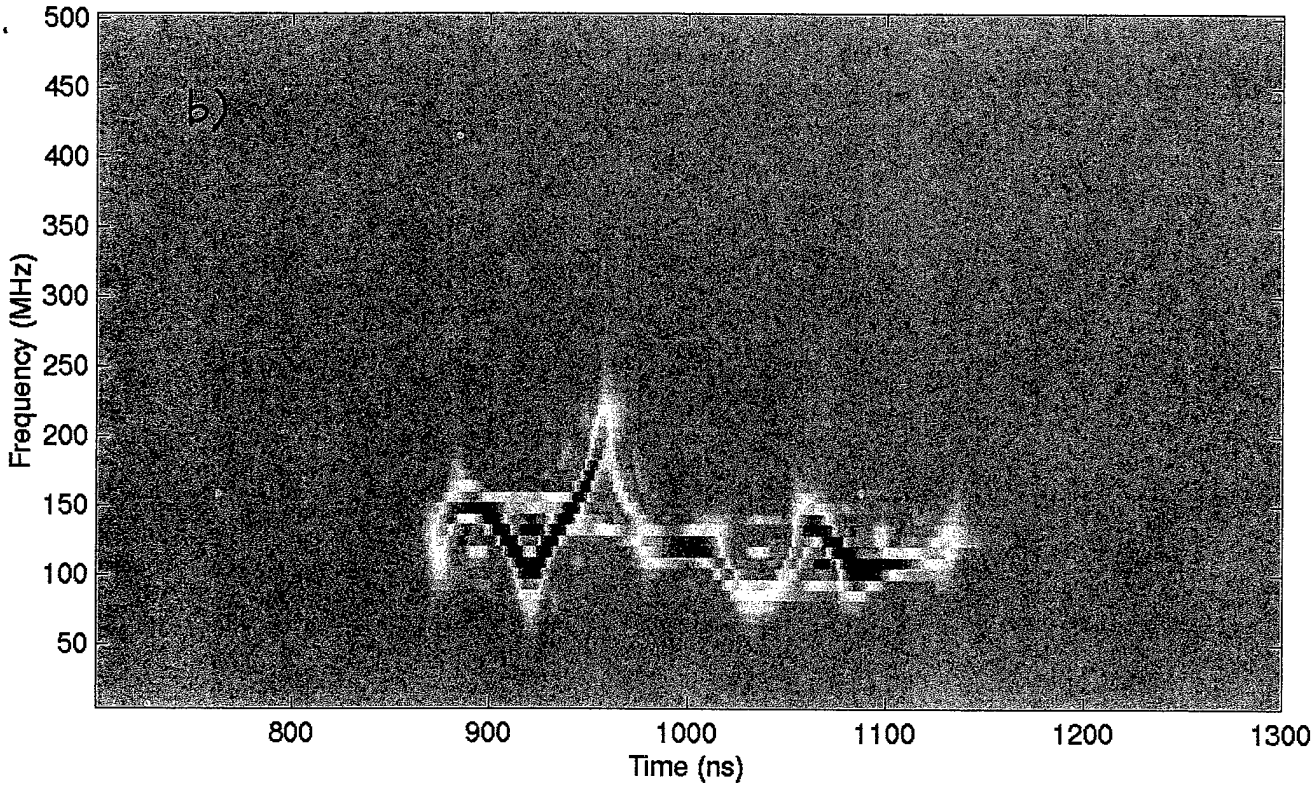
b)
Frequency (MHz)
500
450
400
350
300
250
200
150
100
50
800
900
1000
1100
1200
1300
Time (ns)

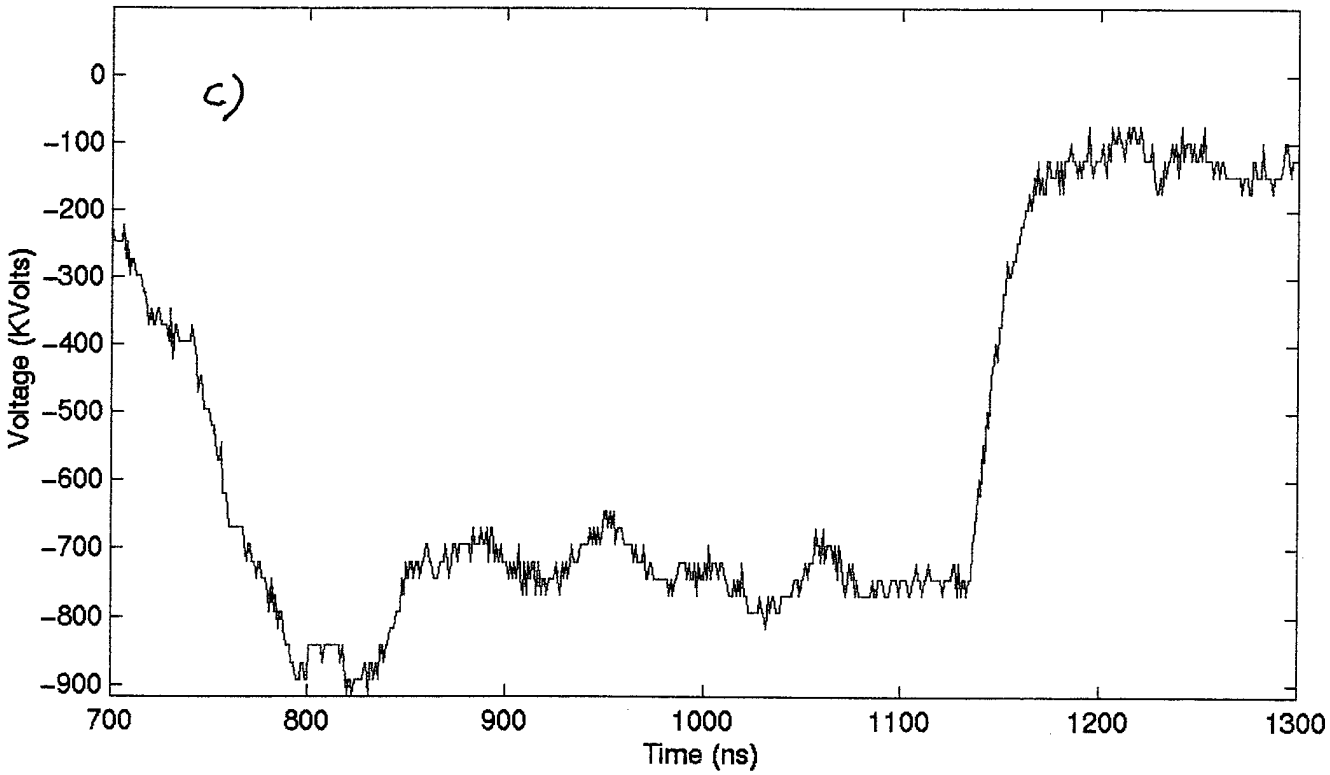
c)
Voltage (KVolts)
0
-100
-200
-300
-400
-500
-600
-700
-800
-900
700
800
900
1000
1100
1200
1300
Time (ns)

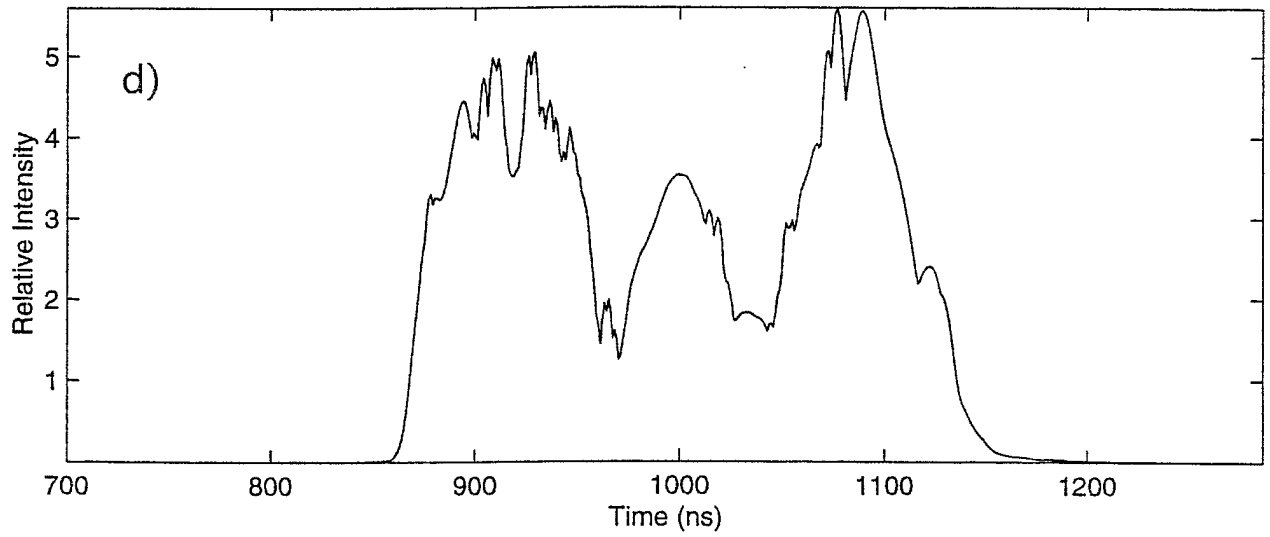
d)
Relative Intensity
5
4
3
2
1
700
800
900
1000
1100
1200
Time (ns)

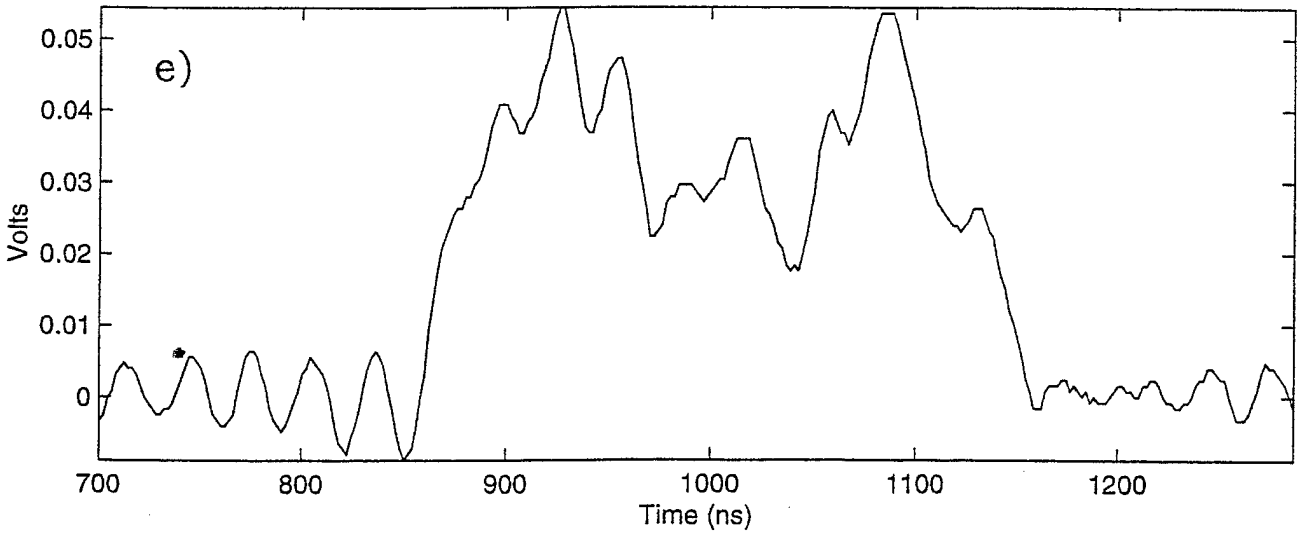
e)
Volts
0.05
0.04
0.03
0.02
0.01
0
700
800
900
1000
1100
1200
Time (ns)

Fig. 2 (cont'd)

Optical Spectroscopy of Plasma in High Power Microwave Pulse Shortening Experiments Driven by a μs e-Beam

Ronald M. Gilgenbach, *Senior Member, IEEE*, Jonathan M. Hochman, *Student Member, IEEE*, Reginald L. Jaynes, William E. Cohen, Joshua I. Rintamaki, Chris W. Peters, Doyle E. Vollers, Y. Y. Lau, and Thomas A. Spencer, *Senior Member, IEEE*

***Abstract*—Microwave pulse shortening experiments have been performed on a rectangular-cross-section (RCS) gyrotron driven by the Michigan Electron Long Beam Accelerator (MELBA) at parameters $V = -800$ kV, $I_{\rm tube} = 0.3$ kA, and pulselengths of 0.5–1 μs. Pulse shortening typically limits the highest (10 MW level) microwave power pulselength to 100–200 ns. Potential explanations of pulse shortening are being investigated, particularly plasma production inside the cavity and at the e-beam-collector. We report the first optical spectroscopy diagnostic measurements inside an operating gyrotron as a means of exploring plasma effects on pulse shortening. Plasma hydrogen H-α line radiation has been characterized in both time-integrated and temporally-resolved measurements and correlated with microwave power/cutoff. Hydrogen is believed to originate from water absorbed on internal tube surfaces in the gyrotron.**

I. Introduction

ONE OF THE most important issues in high power microwave generation is pulse shortening [1]–[7]. Most intense e-beam generators have a pulselength of a few hundred ns, which is too short to fully explore the limits on microwave pulselength. The Michigan Electron Long Beam Accelerator (MELBA) [8] has a pulselength which is adjustable from 200 ns to over 1 μs, at a voltage of -0.8 MV, and current of 1–10 kA. MELBA also incorporates an Abramyan circuit [8] on the Marx generator to flatten the output voltage up to 1.5 μs. This permits investigations of the basic microwave generation mechanisms.

The microwave device under study at the University of Michigan is the rectangular cross section (RCS) gyrotron [9]–[11]. This device has the advantage that the microwave power can be extracted in either of two orthogonal linear polarizations (TE_{10} versus TE_{01}) by adjustment of the solenoidal magnetic field. Further details on the operational characteristics of this RCS gyrotron are presented in another article in this issue [12]. This RCS gyrotron oscillator is a first step toward an active circulator gyrotron traveling wave amplifier [11].

This RCS gyrotron has exhibited microwave pulse shortening which is believed to be caused by plasma. It is difficult to diagnose plasma in a tube which contains both an intense electron beam and high power microwaves. Optical spectroscopy is ideally suited to diagnosis of microwave pulse shortening, since it yields species identification and temporal evolution. We report here the first measurements in which spectroscopic plasma diagnostics have been utilized to characterize plasma emission inside an operating high power, microwave gyrotron as a means of studying microwave pulse shortening.

II. Experimental Configuration

The experimental configuration is depicted in Fig. 1. The cathode electron emission area consists of an annular, roughened, bare aluminum strip; Glyptal is applied to areas where electron emission is to be suppressed. The graphite anode has a three-slotted annular opening. In order to obtain a rotating electron beam, the electron beam is passed through a magnetic cusp (versions I and II described in [12]) of roughly ± 1 kGauss, as shown in Fig. 1(b). The rotating electron beam enters a circular aperture in a rectangular microwave cavity of dimensions 7.2 cm by 5.4 cm, with 21 cm length. The output end of the cavity employs copper strips in the vertical and horizontal direction to adjust the cavity quality factor (Q) of the orthogonal modes (TE_{10} versus TE_{01}). This gyrotron has also employed cavities tapered in one dimension; the cavity tapered in the y dimension (data in Figs. 9 and 10) has dimensions 5.6 cm $\times$ 5.4 cm at the input end verus 7.2 cm $\times$ 5.4 cm at the output end.

Microwave output is directed by rectangular waveguide through an output window into a large chamber lined with microwave absorber. Two cross-polarized, open-ended, S-band waveguides are utilized to detect the microwave power in each of the two orthogonal polarizations.

Plasma optical emission is detected by a fiberoptic bundle placed against the Lucite output window, oriented to view down the gyrotron axis toward the cathode. Inside the Faraday

Manuscript received December 9, 1997; revised March 5, 1998. This paper was presented in part at the International Workshop on High Power Microwave Generation and Pulse Shortening, Edinburgh, U.K., June 1997. This work was supported by the AFOSR-MURI program through a subcontract from Texas Tech University, Northrop Grumman, and the AFOSR-AASERT and AFOSR-DURIP programs. The work of J. I. Rintamaki was supported by a DoE MFET Fellowship.

R. M. Gilgenbach, J. M. Hochman, R. L. Jaynes, W. E. Cohen, J. I. Rintamaki, C. W. Peters, D. E. Vollers, and Y. Y. Lau are with the Intense Energy Beam Interaction Laboratory, Nuclear Engineering and Radiological Sciences Department, University of Michigan, Ann Arbor, MI 48109-2104 USA (e-mail: rongilg@engin.umich.edu).

T. A. Spencer is with the Air Force Research Lab, Phillips Lab, Kirtland AFB, NM 87117 USA.

Publisher Item Identifier S 0093-3813(98)04284-2.

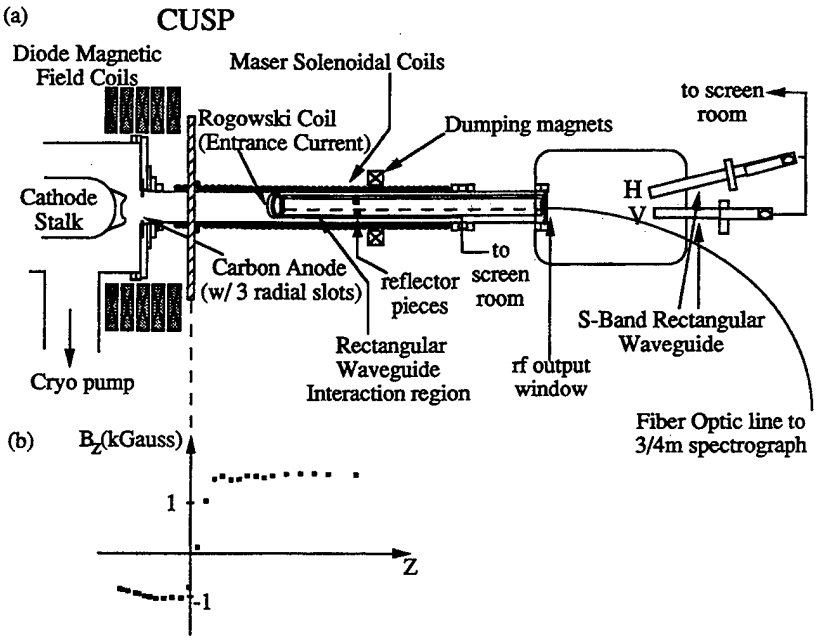

Fig. 1. (a) Experimental configuration for RCS gyrotron. (b) Magnetic field profile of cusp.

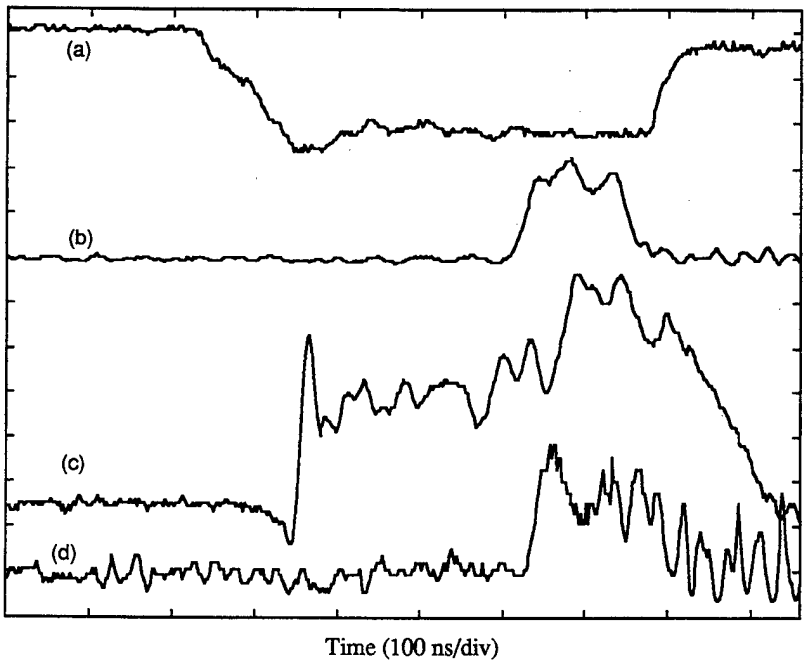

Fig. 2. Experimental data from RCS gyrotron, Cusp I, solenoidal magnetic field of 1.46 kG. (a) Beam voltage (400 kV/div), (b) microwave power (vertical polarization, peak of 9 MW), (c) electron beam current at cavity entrance (40 A/div), and (d) microwave power (horizontal polarization, peak of 30 kW).

cage, the output end of the fiberoptic is directed to the entrance slit of a 0.75 m spectrograph with a gated, intensified, CCD camera system; alternatively, emission from a single spectral line can be measured as a function of time with a photomultiplier tube. Spectra are stored in a personal computer for analysis.

Vacuum pumping was typically performed by means of a single cryopump located under the diode. The ion gauge was located in this pumping port; a second ion gauge was later tested on the collector-end of the tube. A residual gas analyzer (RGA) was connected to the diode chamber by a 3.8-cm diameter, 43-cm long pipe; this accounts for the difference between ion gauge and RGA partial pressures.

III. Experimental Results and Discussion

Experimental RCS gyrotron data signals are presented in Fig. 2. It can be seen that the MELBA voltage pulse is very flat for about 0.4 μs. Cavity entrance current also shows slight diode closure. However, the microwave signal drops off in about 100 ns after peaking at about 9 MW. This pulse shortening behavior is typical of the RCS gyrotron and its cause is the subject of the present investigation.

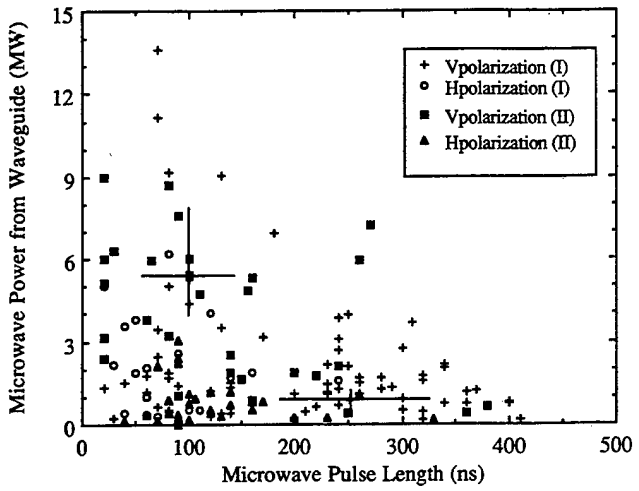

Fig. 3. Microwave power versus pulselength for rectangular cross section gyrotron for two series of experiments with different cusp fields (I and II described in [12]). Pulselengths shown for vertical polarization (V_{pol}) of TE_{10} mode and horizontal polarization (H_{pol}) of TE_{01} mode.

Fig. 3 summarizes the microwave power versus pulselength for the RCS gyrotron. It can be seen that the general trend of pulse shortening with increasing microwave power is observed. These data include shots with resonantly and nonresonantly tuned magnetic fields, which accounts for the large scatter in power. Error bars (standard deviation) have been included for two magnetic fields at which a statistically significant number of shots were taken (8 and 9 shots).

A mass spectrum is shown in Fig. 4, where data was obtained from a residual gas analyzer connected to the MELBA diode (cryopumped without the microwave tube). Table I gives the species composition before [Fig. 4(a)] and after [Fig. 4(b)] a MELBA diode current shot. These data clearly show that water vapor is the major initial impurity (78%) in these experiments, most likely desorbed from metal surfaces by electron beam scraping and dumping at the collector. The post-shot decrease in water concentration (78–53%) and increase in hydrogen (3–18%) is consistent with the electron beam-induced decomposition of water vapor [13].

Spectrally resolved, gated (1 μs), hydrogen H-α emission is presented in Fig. 5. Hydrogen gave the strongest optical emission observed in these spectroscopic data. Small emission peaks from carbon ions are also visible. Aluminum cathode plasma is also observable spectroscopically (Fig. 6), exhibiting neutral atom emission from both the 394.40 nm line and the 396.15 nm line.

Fig. 7(a) and (b) give gated (1 μs), spectroscopic, CCD data from measurements of hydrogen H-α emission versus shot number for comparison with the microwave power. These experimental runs were interesting because data were obtained under two different vacuum conditions, a moderately low tube (diode) pressure of 1.5×10^{-5} torr (6×10^{-6} torr) in Fig. 7(a) and increased tube (diode) pressure of 4×10^{-5} (2×10^{-5} torr) in Fig. 7(b). Regarding the pumping time, prior to lower-pressure shots in Fig. 7(a), (M6185–M6225), the tube/diode were on the roughing pump for about six days, and on the cryopump for 3 h. Before the run on higher pressure shots,

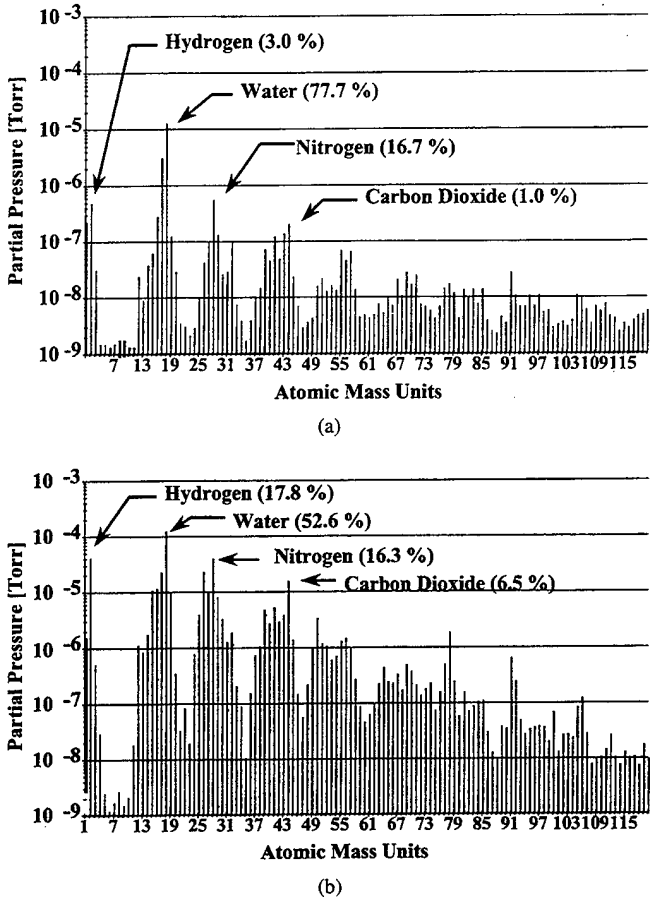

Fig. 4. Residual gas analyzer traces of cryopumped MELBA diode. (a) Before shot and (b) after shot, with gate valve closed immediately.

TABLE I
RESIDUAL GAS ANALYSIS OF CRYO-PUMPED MELBA DIODE

Species	% Before shot	% After shot
Hydrogen	3.0	18
Methane	0.0	1.4
Water	78	53
Nitrogen	17	16
Oxygen	0.3	0.5
NO	0.2	1.4
Argon	0.3	1.2
CO2	1.0	6.5
MP Oil	0.9	2.2
Total Pressure	1.5e-6 Torr	1.4e-5 Torr

Fig. 7(b), (M6226–M6264), the tube/diode were roughing-pumped for 7 days, and cryopumped for one hour. It is believed that the repetition rate is sufficiently low on MELBA that wall-recontamination takes place between shots at these pressures. (Obviously, in a repetitively-pulsed experiment, the water could be conditioned off walls with the e-beam.)

At the lower pressure in Fig. 7(a), there appears to be a stronger correlation [than Fig. 7(b)] between microwave power and the intensity of time-integrated H-α optical emission. Since the higher power shots typically have shorter pulselengths (Fig. 2), these data suggest a connection between pulse shortening and hydrogen plasma optical emission. Fig. 8 is

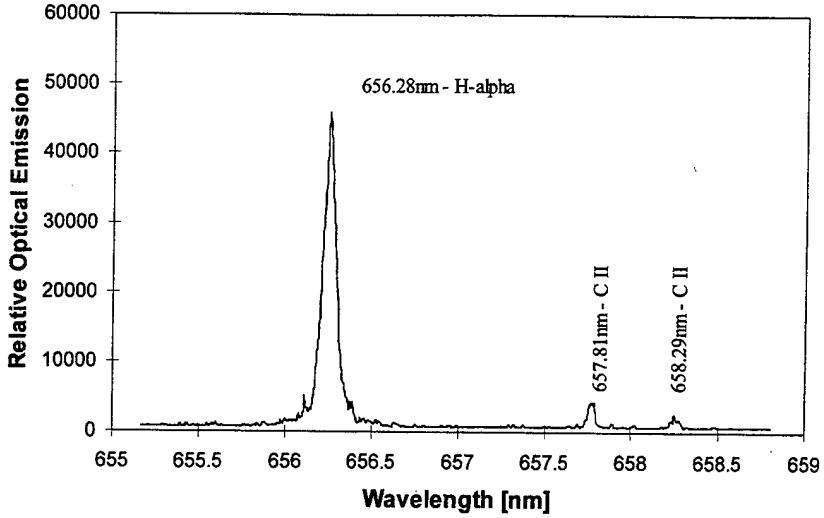

Fig. 5. Gated (1 μs) optical emission spectrum of hydrogen H-α emission line and two carbon lines.

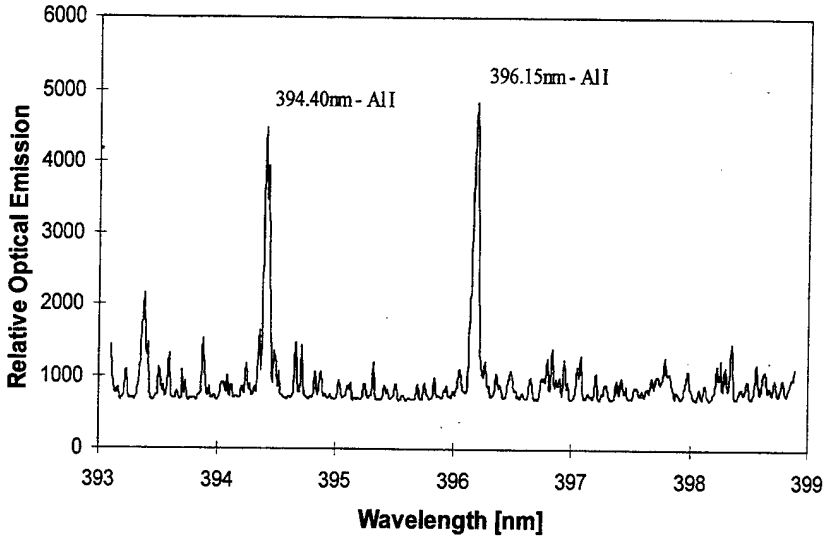

Fig. 6. Gated (1 μs) optical emission spectrum of aluminum from cathode plasma.

a plot of microwave pulselength versus gated H-α optical emission intensity; an inverse correlation is seen over a number of shots.

Figs. 9 and 10 show temporally-resolved H-α emission data versus *e*-beam voltage and microwave power. These data illustrate two types of behavior observed in these experiments. Fig. 9 demonstrates after an initial microwave spike, a gradual reduction of microwave power. The corresponding plasma H-α optical emission shows a gradual increase during the same time interval as the microwave cutoff. It should also be noted that the peak of the plasma H-α optical emission occurs some 600 ns after the initial voltage rise (current turnon). This suggests that the plasma density may be increasing due to the transport of fast hydrogen atoms from ablated wall water (discussed below).

Fig. 10 exhibits a different behavior of microwave cutoff and plasma optical emission. In this type of shot, the high power microwaves show a short (<100 ns), intense (~2.5 MW) burst, followed by a sharp cutoff at about the same time that the plasma H-α optical emission begins. The plasma H-α emission rises rapidly about 500 ns after the voltage rise (current turnon).

These data and other similar pulses strongly suggest that the cutoff of microwave power is closely associated with the onset of hydrogen plasma optical emission. The picture that emerges from these preliminary studies is that the electron beam desorbs and dissociates water vapor from the walls of the tube and collector. Fast (1–10 cm/μs), hydrogen neutral atoms can rapidly fill the waveguide. The high power microwaves could break down the hydrogen into a dense plasma, which cuts off the microwaves.

The fact that there may be an excessive amount of water sticking to any normal surface is well-known in vacuum processes [14]. Water is a highly charged polar molecule which, in the presence of (any) charge imbalance on a free surface, will attach to that surface tenaciously. The water molecules attached to the surface cannot be pumped out readily. In fact, in almost all vacuum systems, water is the

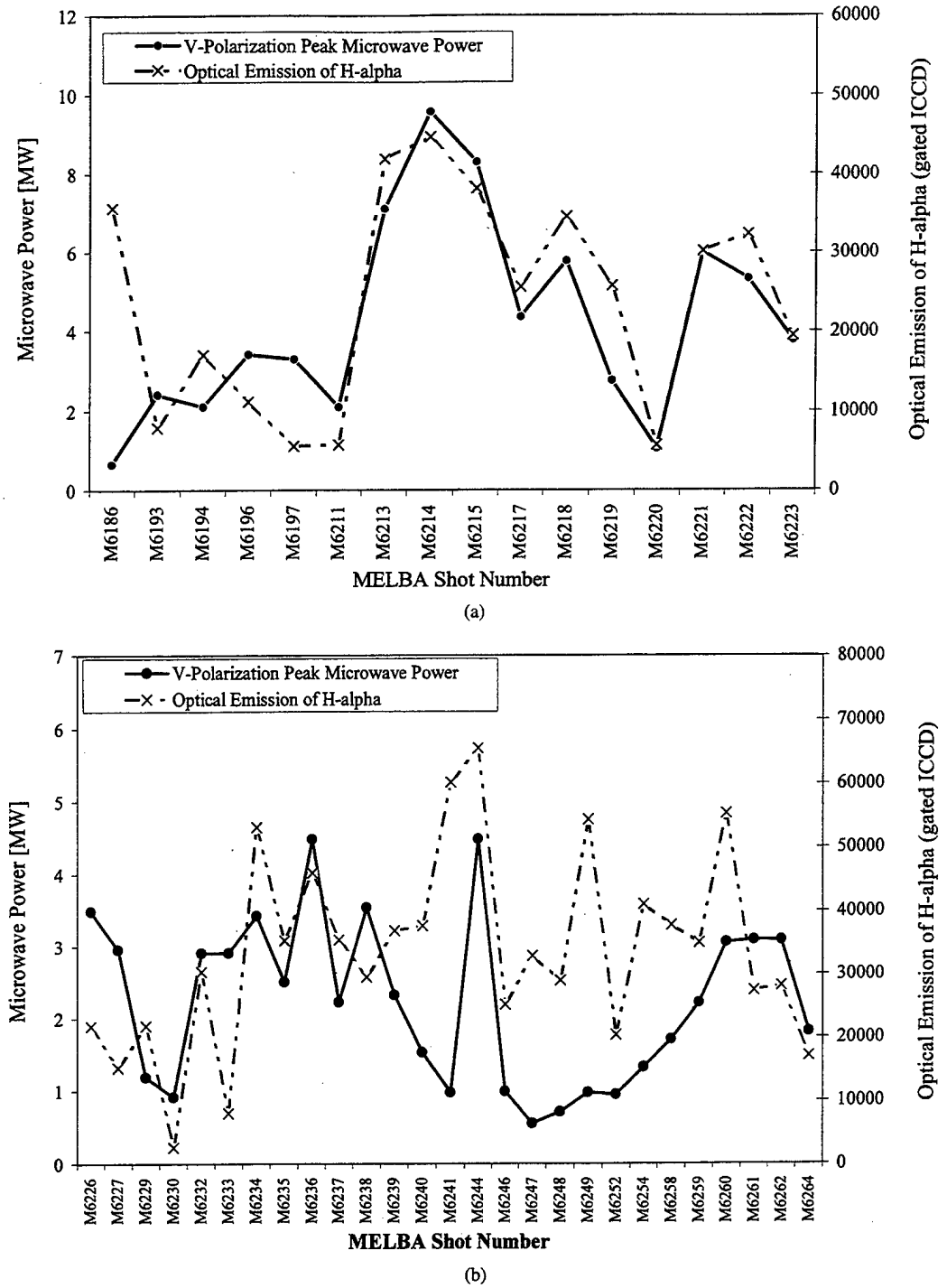

Fig. 7. Hydrogen H-α emission intensity (gated for 1 μs and normalized for gain) and microwave power versus shot number for two different vacuum conditions: (a) tube (diode) pressure of 1.5×10^{-5} torr (6×10^{-6} torr) and (b) tube (diode) pressure of 4×10^{-5} (2×10^{-5} torr).

dominant gas load once the vacuum level falls below a few torr [14]. For a fairly smooth and just normally "wet" surface, there may be as many as 10–20 monolayers of H_2O on the surface with a roughness factor of 10. This yields a surface density reaching 10^{17} water molecules per square centimeter, as inferred from the estimates of [14]. This high concentration of H_2O molecules becomes a natural source of the hydrogen plasma that is thought to be a major culprit for microwave pulse shortening considered in this paper.

The area of the electron beam footprint is about 20 cm^2 and this was taken as the area of the electron beam on the beam dump. It is estimated that this impact area generates about 2×10^{18} water molecules from the wall. Since the ablated wall-neutrals/plasma can have an expansion velocity of 1–10 cm/μs (as in [15]), the (5.4 cm $\times$ 7.2 cm) waveguide could be completely filled in as little as 500 ns. Even assuming that only 4×10^{-5} of these 2×10^{18} molecules (as fast neutrals or plasma in the tail of a few electron volts Maxwellian

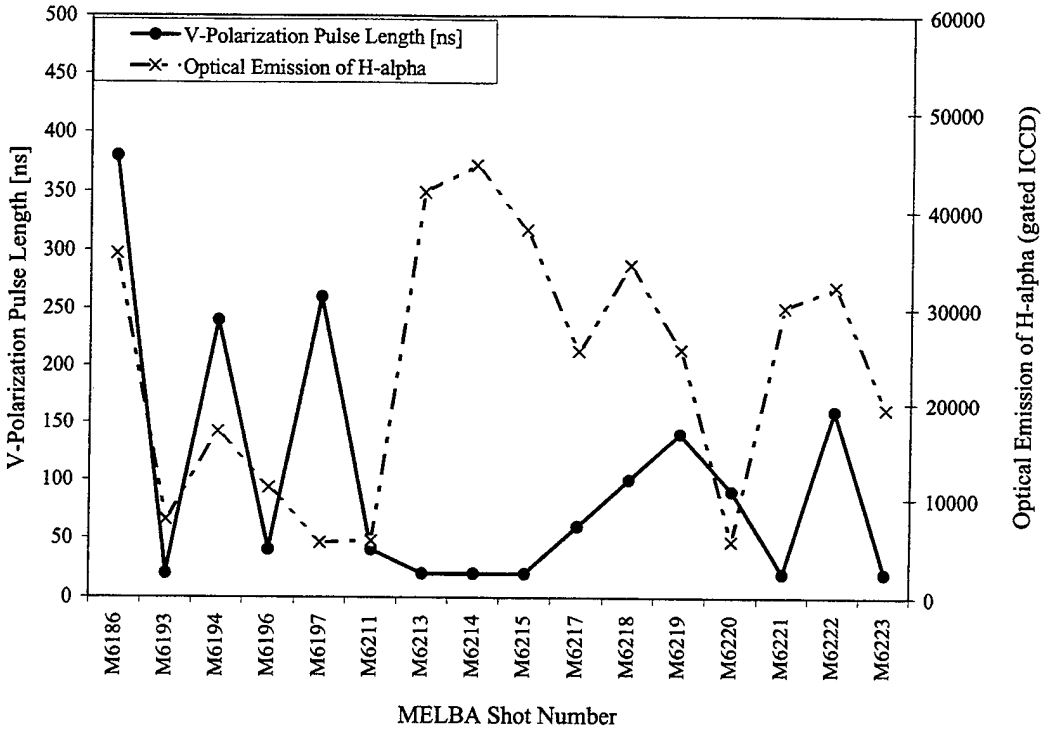

Fig. 8. Hydrogen H-α emission intensity (gated, 1 μs) and normalized for gain; microwave pulselength versus shot number for same shots as Fig. 7(a).

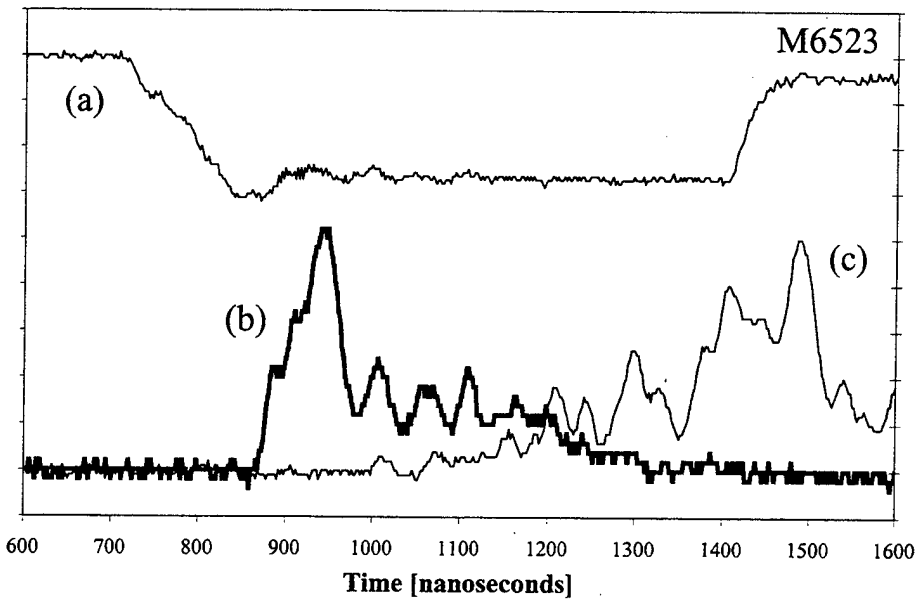

Fig. 9. Temporally resolved signals from MELBA RCS gyrotron shot M6523. Cavity tapered in y dimension, Cusp II. (a) Electron beam voltage (310 kV/div), (b) microwave signal: (vertically polarized, peak power = 2.8 MW), and (c) H-α optical emission signal on photomultiplier tube.

distribution) expand rapidly enough to fill the waveguide volume (over a 10 cm length), this yields a density exceeding 2×10^{11} cm^{-3} or a plasma cutoff frequency of 4 GHz. Data show that many shots have 500 ns time delay from the current-rise to the pulse-cutoff of the microwaves. (The magnetic field does not affect fast-neutral expansion. In the collector, the B field is weak and the dump magnets yield a parallel component of B for plasma expansion, so fast plasma can also readily expand.) These estimates are not meant to be exact; rather, they are intended to illustrate that water liberation and expansion of a only a small fraction of fast-tail particles in the tube is capable of creating a plasma with high enough density to cutoff 2–4 GHz microwaves. Another estimate may be made by referring to [13]. While H_2O is not identified, gas molecules of density as high as 10^{18} cm^{-3} are conjectured to be desorbed near the surface prior to pulse shortening [13]. A tiny fraction of this density, from the fast neutrals or from the Maxwellian tail of a plasma, may account for the plasma density of 2×10^{11} cm^{-3} required to cutoff a frequency of 4 GHz.

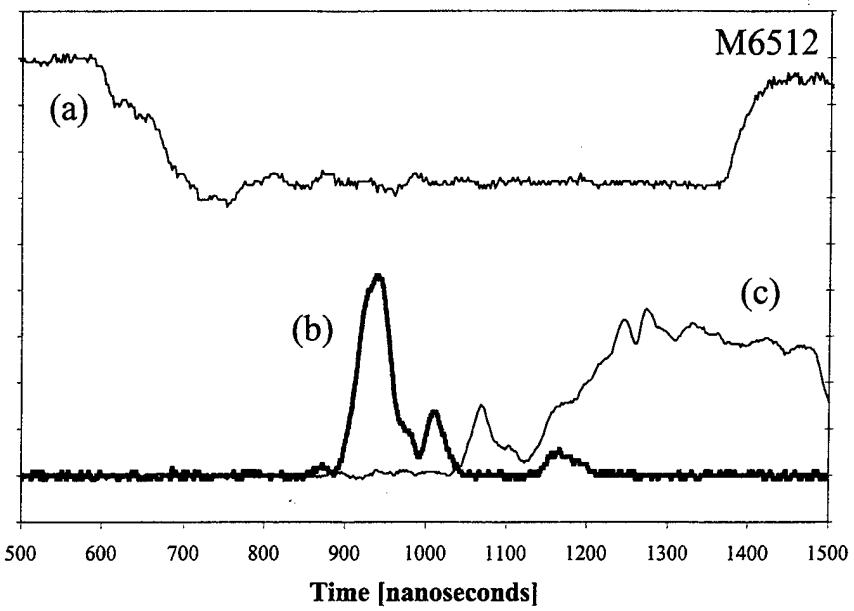

Fig. 10. Temporally resolved signals from MELBA RCS gyrotron shot M6512. Cavity tapered in y dimension, Cusp II. (a) Electron beam voltage (310 kV/div), (b) microwave signal: (vertically polarized, peak power = 2.5 MW), and (c) H-α optical emission signal on photomultiplier tube.

IV. Future Research

Future experiments will elucidate the mechanisms for plasma generation by utilizing fiberoptic probes to obtain spatial resolution of optical emission inside the microwave tube (cavity versus collector). Experiments can also measure plasma optical emission to test the relationship between plasma and e-beam scraping by spoiling of the microwave generation.

Other experiments will explore protocols for plasma processing the inside of microwave tubes in order to eliminate water vapor and other contaminants.

References

[1] F. J. Agee, "Basic research in high power microwaves: The US program," *Dig. Technical Papers Int. Workshop High Power Microwave Generation and Pulse Shortening*, Edinburgh, U.K., June 10–12, 1997, p. 1.

[2] R. M. Gilgenbach, J. M. Hochman, R. Jaynes, W. Cohen, J. I. Rintamaki, Y. Y. Lau, and T. A. Spencer, "High power microwave pulse shortening experiments driven by a microsecond electron beam," *Dig. Tech. Papers Int. Workshop on High Power Microwave Generation and Pulse Shortening*, Edinburgh, U.K., June 10–12, 1997, p. 109.

[3] D. Price and J. Benford, "General scaling of pulse shortening in explosive-emission-driven microwave sources," this issue, pp. 256–262.

[4] D. M Goebel, "Pulse shortening causes in high power BWO and TWT microwave sources," this issue, pp. 263–274.

[5] R. B. Miller, "Pulse shortening in high peak power reltron tubes," *SPIE*, vol. 2843, p. 2–13, 1996.

[6] M. T. Walter, R. M. Gilgenbach, J. W. Luginsland, J. M. Hochman, J. I. Rintamaki, R. L. Jaynes, Y. Y. Lau, and T. A. Spencer, "Effects of tapering on gyrotron backward wave oscillators," *IEEE Trans. Plasma Sci.*, vol. 24, pp. 636–647, 1996.

[7] T. A. Spencer, C. E. Davis, K. J. Hendricks, F. J. Agee, and R. M. Gilgenbach, "Results from gyrotron backward wave oscillator experiments utilizing a high current, high voltage annular electron beam," *IEEE Trans. Plasma Sci.*, vol. 24 pp. 630–635, 1996.

[8] R. M. Gilgenbach *et al.*, "Microsecond electron beam diode closure experiments," in *Proc. Fifth IEEE Pulsed Power Conf.*, June 10–12, 1985, p. 126, IEEE Catalog Number 85C 2121-2.

[9] D. J. Radack, K. Ramaswamy, W. W. Destler, and J. Rodgers, "A fundamental mode, high power, large orbit-gyrotron using a rectangular interaction region," *J. Appl. Phys.*, vol. 73, p. 8139, 1993.

[10] R. M. Gilgenbach *et al.*, "Rectangular cross section gyrotron," in *Proc. Infrared Millimeter Waves Conf.*, Orlando, FL, 1995.

[11] Y. Y. Lau, L. R. Barnett, and J. M. Baird, "An active circulator-gyrotron traveling-wave amplifier," *IEEE Trans. Electron Devices*, vol. ED-31, p. 337, 1984.

[12] J. M. Hochman, R. M. Gilgenbach, R. L. Jaynes, J. I. Rintamaki, Y. Y. Lau, W. E. Cohen, C. Peters, and T. A. Spencer, "Polarization control of microwave emission from high power rectangular cross-section gyrotron devices," this issue, pp. 383–392.

[13] G. A. Mesyats, "The problem of pulse shortening in relativistic microwave generators," in *High Power Microwave Generators and Applications*, D. Akulina, E. Sindoni, and C. Wharton, Eds. Bologna, Italy: Societa Italiana di Fisica, 1992.

[14] J. Harvell and P. Lessard, "Managing water vapor in vacuum process," *Semicond. Int.*, June 1991.

[15] R. M. Gilgenbach and P. L. G. Ventzek, "Dynamics of excimer laser—Ablated aluminum-neutral-atom plume measured by dye-laser-resonance-absorption photography," *Appl. Phys. Lett.*, vol. 58, p. 1597, 1991.

Ronald M. Gilgenbach (S'73–M'74–SM'92) received the B.S. and M.S. degrees in 1972 and 1973, respectively, from the University of Wisconsin, Madison, and the Ph.D. degree in electrical engineering from Columbia University, New York, NY, in 1978.

He is currently Professor in the Nuclear Engineering and Radiological Sciences Department and in the Applied Physics Program at the University of Michigan, Ann Arbor. He gained several years of industrial experience at Bell Labs. From 1978 to 1980, he worked as a contractor at the Naval Research Laboratory, Washington, DC, where he was involved in research and development on the first, long-pulse, 35-GHz gyrotron for plasma heating. He performed experiments on the ISX-B tokamak at Oak Ridge National Laboratory, which represented the first gyrotron electron cyclotron heating experiments on a tokamak in the United States. He joined the faculty of the University of Michigan in 1980 and became Director of the Intense Energy Beam Interaction Laboratory, a post he still holds. His research at Michigan has concentrated on the physics and applications of electron beams and microwaves, as well as laser-plasmas, laser diagnostics, and industrial materials processing. He has had research interactions with scientists at Phillips Lab, Sandia National Labs, Northrop-Grumman, General Motors Research Labs, Los Alamos National Lab, Fermilab, and NRL.

Dr. Gilgenbach is secretary and past member of the Executive Committee of the IEEE Plasma Sciences and Applications Technical Committee. He is a Fellow of the American Physical Society and received the 1997 Plasma Sciences and Applications Award from the IEEE PSAC.

Jonathan M. Hochman (S'97) was born in Chattanooga, TN, in 1965. He received the B.S. degree in chemistry from the University of North Carolina, Chapel Hill, in 1987. After serving as a Nuclear Trained Engineering Officer aboard the U.S.S. Long Beach (CGN 9), he received both the M.S. degree in nuclear engineering and the M.S. degree in electrical engineering in 1995 and 1997, respectively, from the University of Michigan, Ann Arbor, where he is currently pursuing the Ph.D. degree in nuclear engineering.

Since 1993, he has worked in the Intense Energy Beam Interaction Laboratory at the University of Michigan. His research at Michigan has concentrated on the application of electron beams to generate high power microwaves in different gyrotron devices and on electron beam dynamics.

Mr. Hochman is a member of the APS, ANS, and SPIE.

Reginald L. Jaynes was born in Fort Eustus, VA, in 1971. He received the B.S. degree in engineering physics in 1994 and the M.S. degree in electrical engineering in 1997, both from the University of Michigan, Ann Arbor. He is currently pursuing Ph.D. degree in electrical engineering at the University of Michigan.

His research interests include the generation of high power microwaves and coherent radiation.

William E. Cohen was born in St. Louis, MO, in 1973. He received the B.S. and M.S. degrees in nuclear engineering from the University of Michigan, Ann Arbor, in 1995 and 1997, respectively. He is currently pursuing the Ph.D. degree in nuclear engineering at the University of Michigan.

While working toward his undergraduate degree, he worked at Argonne National Laboratory-West, Lawrence Livermore National Laboratory, and Electricite de France (Clarmart, France). He presently works in the Intense Energy Beam Interaction Laboratory, University of Michigan, on plasma spectroscopy of high power gyrotrons. During his graduate work he has also worked at the Fraunhofer Resource Center on laser welding of aluminum.

Mr. Cohen has received a graduate scholarship from the American Nuclear Society and honorable mentions from the DOE Magnetic Fusion Energy Technology and DoD Fellowship Programs. He has also received a Distinguished Leadership Award from the University of Michigan College of Engineering.

Joshua I. Rintamaki was born in 1972 in Affton, MO. He received the B.S. and M.S. degrees in nuclear engineering from the University of Michigan, Ann Arbor, in 1994 and 1996, respectively. He is currently pursuing the Ph.D. degree in nuclear engineering at the University of Michigan.

He has worked at Lawrence Livermore National Laboratories (LLNL) in the summer of 1994, and at Sandia National Laboratories (SNL) in the summer of 1995. He is supported by a Fusion Energy Science DOE Fellowship. His main research interests include plasma processing of high voltage surfaces, high-power microwave generation, and spectroscopy of high voltage beam systems.

Chris W. Peters hails from Oscoda, MI. He served in the U.S. Navy on board the USS Barbey (FF-1088) and USS Fanning (FF-1076) as a Machinist's Mate. He then received the B.S. degree in nuclear engineering from the University of Michigan, Ann Arbor, in 1996. He is currently pursuing the Ph.D. degree in nuclear engineering at the University of Michigan.

Doyle E. Vollers received the B.S.E.E. degree from Michigan Technological University, Houghton, in 1990. He is currently pursuing the M.S.E.E. degree at the University of Michigan, Ann Arbor, specializing in pulsed power.

From 1990 to 1997, he served as a Flight Safety Officer in various U.S. Air Force engineering positions.

Y. Y. Lau, for a photograph and biography, see this issue, p. 234.

Thomas A. Spencer (M'94–SM'95) received the B.S. degree in nuclear science from the Virginia Polytechnic Institute and State University, Blacksburg, in 1986, and the M.S.E. and Ph.D. degrees in nuclear engineering from the University of Michigan, Ann Arbor, in 1988 and 1991, respectively.

He joined the High Power Microwave (HPM) Source group at the Phillips Laboratory (Air Force Research Lab), Kirtland AFB, NM, in 1991, where his present research activities include work on gyrotron backward wave oscillators, relativistic klystron amplifiers, cross-field devices, plasma effects on HPM sources, diode physics, novel cathodes, and RF atmospheric breakdown.

Polarization Control of Microwave Emission from High Power Rectangular Cross-Section Gyrotron Devices

Jonathan M. Hochman, *Student Member, IEEE,* Ronald M. Gilgenbach, *Senior Member, IEEE,* Reginald L. Jaynes, Joshua I. Rintamaki, Y. Y. Lau, William E. Cohen, Chris W. Peters, and Thomas A. Spencer, *Senior Member, IEEE*

Abstract— **Results are summarized of experiments on a gyrotron utilizing a rectangular-cross-section (RCS) cavity region. The major issue under investigation is polarization control of microwave emission as a function of magnetic field. The electron beam driver is the Michigan Electron Long Beam Accelerator (MELBA) at parameters: V =0.8 MV, I_{diode} =1–10 kA, I_{tube} =0.1–0.5 kA, and $t_{e\text{-beam}}$ =0.4–1.0 μs. The annular e-beam is spun up into an axis-encircling beam by passing it through a magnetic cusp prior to entering the RCS interaction cavity. Experimental results show a high degree of polarization in either of two orthogonal modes as a function of cavity fields. The RCS gyrotron produced peak powers of 14 MW in one polarization (TE_{10}) and 6 MW in the cross-polarized mode (TE_{01}). Electronic efficiencies for this device reached as high as 8% with transverse efficiency of 16%. Experimental results on the beam alpha ($\alpha = V_{\perp}/V_{//}$) diagnostics, where alpha is the ratio of the e-beam's transverse velocity to its parallel velocity, agree well with the single electron trajectory code. MAGIC code results are in qualitative agreement with microwave measurements. Microwave emission shifts from the dominant fundamental mode polarization ($TE_{10}\square$), to the next higher order mode polarization ($TE_{01}\square$) as the solenoid magnetic field is raised from 1.4–1.9 kGauss. Frequency measurements using heterodyne mixers support mode identification as well as MAGIC code simulations.**

I. Introduction

GYROTRON devices have been shown to be efficient and high power sources of microwave radiation [1]–[9]. A long-pulse, high power gyrotron device has significant applications to radar systems, plasma heating in tokamaks, and other areas requiring rf drive power such as supercolliders [1]–[4], [9]–[11]. Control of the linearly polarized microwave emission might be useful for a rapid scanning radar or perhaps in fusion plasma startup (X-wave) and heating (O-wave).

A great deal of research on gyrotron devices has been concentrated on small-orbit gyrotrons, some generating up to 1 MW CW and from 30 to 250 MW for short pulses (μs–ns) [8]. However, large-orbit (or axis encircling) microwave devices offer several attractive features, including operation at lower magnetic fields with high-harmonic capabilities [7], [12]–[14]. Most configurations for gyrotrons are cylindrical cavities that are azimuthally symmetric. Cylindrical waveguides with TE_{01}^{o} or TE_{11}^{o} circular output are a convenient geometry for analysis in rotating relativistic electron beams [15]. However, using an interaction structure with a rectangular cross section (RCS) offers several potential advantages [15]. Waveguide microwave output is linearly polarized; therefore, a mode converter from cylindrical to rectangular polarization is not required. Previous experiments elsewhere with RCS large-orbit gyrotrons have demonstrated 40 MW pulses (75 ns) with efficiencies of about 16%, and very short duration pulses (tens of ns) of 100 MW [15]. For cylindrical geometry, large-orbit gyrotrons, power levels in the range of 500–1000 MW have been reported [13].

Polarization control of high power microwaves is another advantage of RCS gyrotrons. This concept could be used in the active-circulator-gyrotron, which operates as a traveling wave amplifier in an almost square waveguide, injecting an input signal of the $TE_{01}(\square)$ form, but amplifying an output wave in the form of the $TE_{10}(\square)$ mode [16], [17]. The experiments reported here demonstrate polarization control in the large-orbit RCS gyrotron oscillator [18]. By control of the magnetic fields on both sides of an asymmetric magnetic cusp, and on the interaction cavity, we have demonstrated the ability to shift high-power radiation polarization between the $TE_{10}(\square)$ mode and the $TE_{01}(\square)$ mode.

II. Experimental Description

The RCS gyrotron at the University of Michigan is designed to operate in the S-band (2–4 GHz). MELBA generates an electron beam with the following parameters: voltage = 0.7–0.8 MV, diode current = 1–10 kA, tube current = 0.1–0.5 kA, and pulselength = 0.5–1.0 μs, with flattop voltage provided by an Abramyan-type compensation stage over 1 μs.

The experimental configuration of the RCS gyrotron is exhibited in Fig. 1. An annular electron beam of radius 2.25

Manuscript received September 15, 1997; revised March 3, 1998. This paper was presented in part at the International Workshop on High Power Microwave Generation and Pulse Shortening, Edinburgh, U.K., June 1997. This research was supported by the Air Force Office of Scientific Research, Multidisciplinary University Research Initiative (MURI) through a Texas Tech University subcontract, Air Force Research Lab, Northrop Grumman Corp., and the AFOSR-sponsored MAGIC Code User's Group, administered by Mission Research Corp. J. M. Hochman was supported by an AFOSR Augmentation Award for Science and Engineering Research Training (AASERT). J. I. Rintamaki was supported under a DoE MFET Graduate Fellowship.

J. M. Hochman, R. M. Gilgenbach, R. L. Jaynes, J. I. Rintamaki, Y. Y. Lau, W. E. Cohen, and C. W. Peters are with the Intense Energy Beam Interaction Laboratory, Nuclear Engineering and Radiological Sciences Department, University of Michigan, Ann Arbor, MI 48109-2104 USA (e-mail: rongilg@engin.umich.edu).

T. A. Spencer is with the Air Force Research Laboratory, Kirtland AFB, NM 87117-5776 USA.

Publisher Item Identifier S 0093-3813(98)04295-7.

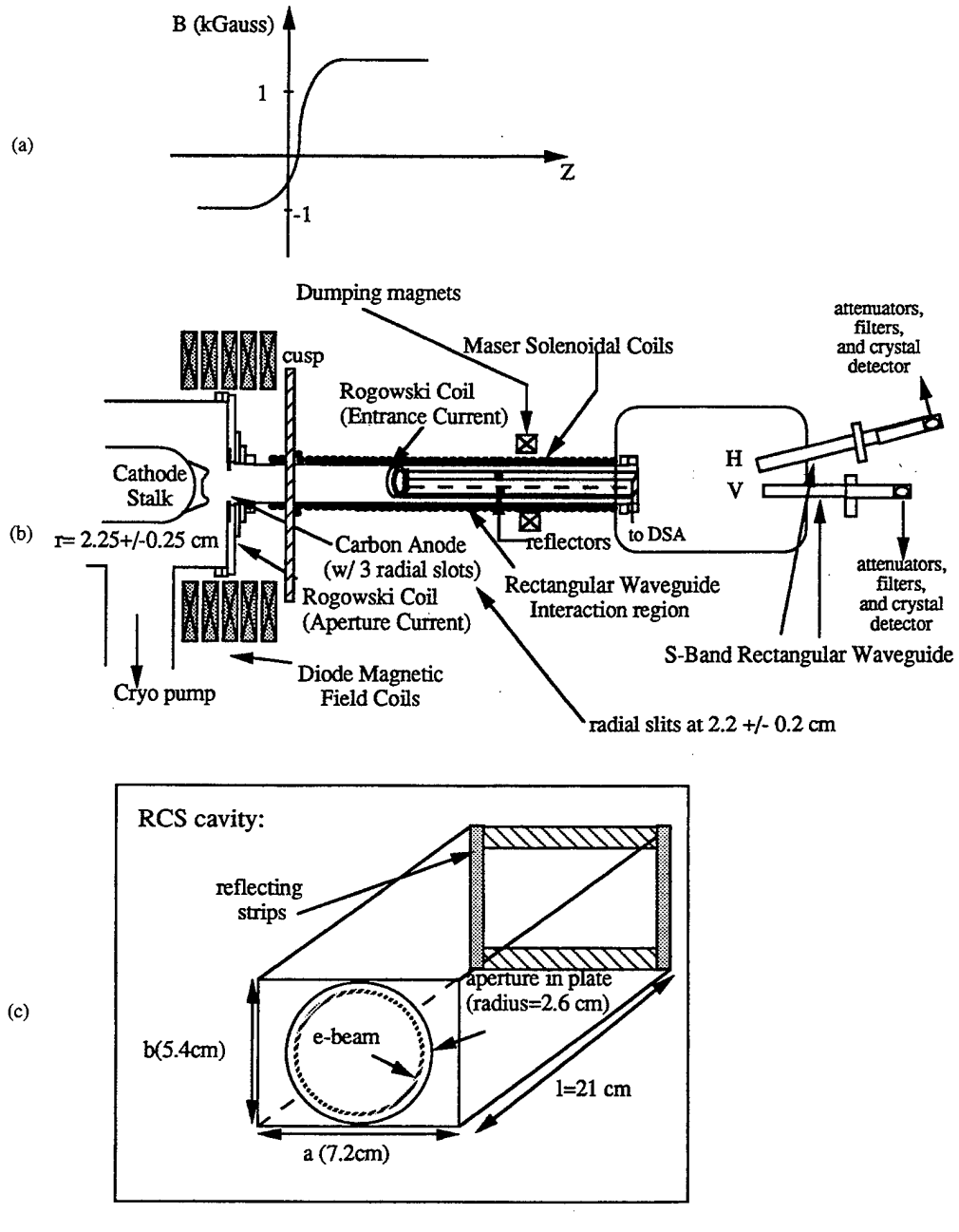

Fig. 1. Experimental configuration for RCS gyrotron measurements. (a) Magnetic field profile as a function of distance. (b) Experimental set-up for microwave measurements. (c) Rectangular cross-section cavity interaction region, starting at 28.5 cm from the anode.

$\pm$ 0.25 cm is produced by explosive emission of an exposed aluminum, annular ring on a glyptal-coated cathode. This cathode consists of a glyptal-coated hemispherical-end cathode stalk with an aluminum tip formed into an annular ring. The graphite anode is located 10.7 cm from the end of the cathode, and has an annular, three-slotted aperture of radius 2.2 $\pm$ 0.2 cm for beam extraction into the transport tube. Large, pulsed, magnetic field coils immerse the diode chamber in a solenoidal field that can be varied from 0.7–3.2 kGauss. The extracted e-beam is passed through a magnetic cusp, defined by a 1.9 cm-thick steel plate. The magnetic field coils on each side of the cusp are controlled by different capacitor banks. After the cusp, the axis-encircling beam travels through the transport chamber, a stainless-steel drift tube surrounded by solenoid coils that are pulsed by one of the capacitor banks controlling the cusp. The magnetic field on the anode side of the cusp is controlled by the capacitor bank maintaining the diode field. A typical magnetic field profile is shown in the experimental configuration [Fig. 1(a)].

Inside the transport tube, the beam interacts with the RCS cavity [Fig. 1(c)] with dimensions of 7.2 cm $\times$ 5.4 cm, which is made by modifying and joining two sections of S-band waveguide. The cavity entrance is 28.5 cm from the anode. The entrance of the cavity has a circular aperture of 2.6 cm radius. The exit of the interaction cavity region has removable copper strips (1 cm $\times$ 7.2 cm and 1 cm $\times$ 5.4 cm) at 21 cm

downstream of the entrance, which are used for varying the cavity Q. The e-beam is dumped to a wall after leaving the interaction region.

Beam current extracted through the anode is measured by a Rogowski coil, and another such coil measures the current prior to the entrance to the RCS cavity. Approximately 500 A of e-beam current exits the anode and 250 A current enters the interaction cavity. A B-dot loop measures the accelerator cathode stalk current. For transported current measurements, the dumping magnets are removed and a graphite collector with a Pearson current transformer are placed at the exit of the RCS cavity.

Microwave output is directed through waveguide of the same transverse dimensions as the interaction cavity. A large chamber lined with microwave absorber is located at the end of the waveguide. Two S-band waveguides, whose wide dimensions are oriented perpendicular to each other at the end of the chamber, are used to collect the high power microwave emissions. The fraction of the total power measured in each of the S-band waveguides was determined by measurements utilizing an HP8722D network analyzer which was swept over the S-band frequency range to determine the attenuation. The waveguides have thin copper wires across the long dimensions to prevent cross-polarized microwave electric fields from entering the waveguide. Microwave signals from directional couplers are transmitted to a Faraday cage via RG-214/U Type E15402 coaxial cable. Attenuators, low pass filters, and calibrated crystal detectors (HP8470B) are used to measure total waveguide power in both waveguide orientations. Frequency spectra are diagnosed by use of two heterodyne mixer systems. Two different microwave oscillators (HP8350B sweep oscillator with a HP83590S RF plug-in and General Radio microwave oscillator) are sources for the mixers' local oscillators, and the rf source from the gyrotron is from an incoming coaxial line. The incoming line uses attenuators, a 4-GHz low pass filter, and a 3 dB power splitter prior to transmission to the two mixers (Minicircuit 15 542 type). The mixer signals are directed to a digital signal analyzer (Tektronix DSA-602) where fast Fourier transforms (FFT's) are computed for frequency spectra. Cold testing of the RCS cavity with an HP8722D network analyzer confirms the cavity resonance frequencies measured by the mixers.

For electron beam diagnostics, the beam alpha ($\alpha = V_\perp/V_{//}$) is measured after going through the cusp by radiation darkening of a glass plate [18], [20]. Alpha is the ratio of the velocity in the transverse dimensions to the velocity in the direction of propagation. A relativistic single-particle-orbit computer code is used to compare the spatial distributions of e-beam trajectories with the witness plates. The anode aperture is changed to eight, 1-mm diameter beamlet holes at a radius of 2.25 cm for these measurements. Twenty shots using MELBA are taken to expose the radiation darkened-patterns on the glass.

III. Experimental Data, Simulation Results, and Discussion

Experiments were conducted in which the microwave powers in the two waveguide orthogonal polarizations ($TE_{10}(\square)$ versus $TE_{01}(\square)$) were measured and compared as function of the magnetic field. From the dispersion relations (Fig. 2) one expects the magnetic field of 1.5 kG to couple most strongly to the lowest order mode polarization, TE_{10}. Conversely, the higher cavity magnetic field of 1.9 kG should couple most strongly to the orthogonally polarized TE_{01} mode, since the $TE_{10}(\square)$ mode in Fig. 2 has an axial wavelength too long ($k_z = 0$) to be fitted in the rectangular cavity.

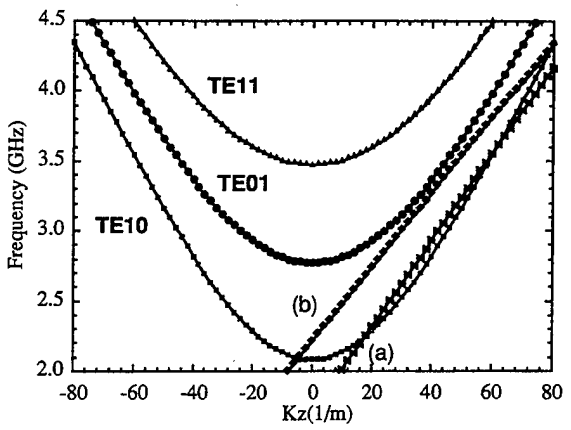

Fig. 2. Waveguide and e-beam-cyclotron-wave dispersion relations for the modied S-band waveguide. (a) e-beam-cyclotron-wave for alpha $(V_\perp/V_{//}) = 1.0, B = 1.5$ kGauss. (b) e-beam-cyclotron-wave for alpha $= 1.3$, $B = 1.95$ kGauss.

Cold testing of the rectangular cross section cavity was performed by inserting a small loop antenna into the experimental cavity near one wall, but axially in the center. Using a HP8722D network analyzer sweeping different frequency ranges, resonant frequencies are determined by dips in the $S11$ scattering parameter. Fig. 3 shows one such sweep of the network analyzer between 2 and 4 GHz. Four different cavity modes appeared on this sweep. These cold test measurements observed the $TE_{101}, TE_{011}, TE_{111}$, and TE_{201} (or TE_{104}) modes. The cold cavity Q was measured to be approximately 500 for the fundamental mode (TE_{101}) at 2.15 GHz, and approximately 650 for the orthogonal TE_{011} mode at 2.88 GHz [21]. As will be discussed below, all four modes appeared during e-beam operation of the RCS gyrotron. Additionally, during e-beam tests, the TE_{102} mode (as opposed to the TE_{101} mode) appeared. The TE_{102} mode did not appear during cold tests since it has a field null at the axial center of the cavity where the probe was placed.

Experimental RCS gyrotron emission data are shown in Fig. 4. These data were taken at a field of 1.5 kGauss. The voltage pulse in Fig. 4(a) shows an initial overshoot which is followed by a flattop voltage of approximately 800 keV for the remainder of the 500 ns pulse. The current measured at the entrance of the RCS cavity in Fig. 4(b) peaks at 255 A. Transported current measurements showed that the current exiting the anode aperture averaged 470 A. Current entering the RCS cavity averaged approximately 200 A, and current measured at the output of the cavity averaged approximately 160 A. The peak microwave power for the TE_{01} horizontally polarized wave in this shot was 0.05 MW [Fig. 4(c)], which is in stark contrast to the peak power measured for the fun-

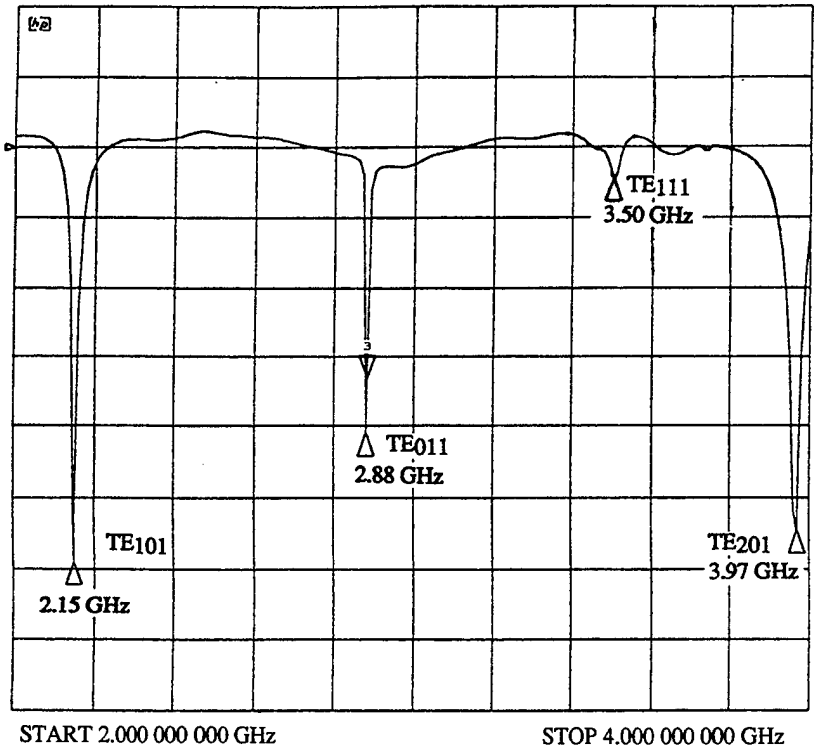

Fig. 3. Cold test frequency sweep of the RCS cavity using an HP8722D network analyzer. The sweep was conducted from 2–4 GHz with peaks corresponding to the TE_{101}, TE_{011}, TE_{111}, and TE_{201} modes. The TE_{101} mode at 2.15 GHz had a Q of approximately 500, and the TE_{01} mode at 2.88 GHz had a Q of approximately 650.

damental TE_{10} mode at 11 MW [Fig. 4(d)]. The polarization power ratio, $\mathrm{Pwr}(TE_{10})/\mathrm{Pwr}(TE_{01})$, was thus approximately 225 for this shot, favoring the dominant fundamental mode. Fig. 4(e) is the mixer signal and Fig. 4(f) is the FFT of the mixer signal. The peak power corresponds to a frequency of 2.16 GHz. This compares well with cold test results for the TE_{101} mode peak at 2.15 GHz.

In order to interpret the data, the beam alpha is required. Beam diagnostics were completed by radiation darkening of glass plates. Fig. 5(a) shows the model for measurements, and Fig. 5(b) shows how the radiation darkening from one beamlet compared with a relativistic single particle trajectory computer code. The cross-hatched area shows where the radiation darkening took place, and the individual dots show where the code predicted darkening. The program numerically integrates relativistic equations of motion of a single particle. The particle in the code is started at the anode and stopped at an axial distance corresponding to the position of the glass witness plate. One thousand particles are used, given the same initial position (radius, θ), but different initial directions in velocity with spread in angles less than 5° from the axis. This spread is set such that beta (V/c) is equal to 0.914. By assuming the beam trajectory is composed of cyclotron orbits [20], one can calculate the beam alpha $(V_\perp/V_{//})$ using

$$\alpha = 1/(\sqrt{(\gamma\beta mc/RqB)^2 - 1}) \quad (1)$$

where γm is the relativistic mass, βc is the beam velocity, R is the Larmor radius, q is the charge on an electron, and B is the magnetic field. Experimentally, the beam alpha was measured to be approximately one at a magnetic field of 1.5 kGauss. The code determined the alpha range between 0.6 to as high as 3.5 with an average range of 1.0–1.2, which is in good agreement with the experiment. When the magnetic field was raised to 1.95 kGauss, the experimental average beam alpha appeared to be on the order of ~1.3–1.5.

The microwave power measurements for two cusps are shown in Fig. 6. The two cusps (cusp I and cusp II) are similar in design (see Fig. 1) with exception that cusp II had improved azimuthal symmetry of the magnetic field in the cusp region. Radiation darkening on glass plates, as done for beam alpha measurements, showed cusp II e-beams to be more annular and uniform than cusp I. Furthermore, results utilizing cusp II were more reproducible than cusp I. Improvements in the magnetic cusp did not have a significant impact on the current entering the RCS interaction cavity. The average current entering the cavity from cusp I was approximately 200 ± 65 A, and the average current entering the cavity from cusp II was approximately 188 ± 37 A. In both cusps the current entering the RCS cavity was slightly higher on average at lower magnetic fields (~1.5 kGauss). While cusp II produced less current entering the RCS cavity, radiation darkening on glass plates showed a better quality beam with lower energy spread and hence, a more efficient large orbit gyrotron on average. In cusp I [Fig. 6(a)], microwave power as high as 14 MW was measured in the fundamental mode (TE_{101}) while negligible power was measured in the orthogonal mode; this was performed at a magnetic field of 1.48 kGauss on the interaction cavity. The diode was maintained at approximately 1 kGauss during all of these measurements. Furthermore, frequency spectra showed that at low fields the fundamental

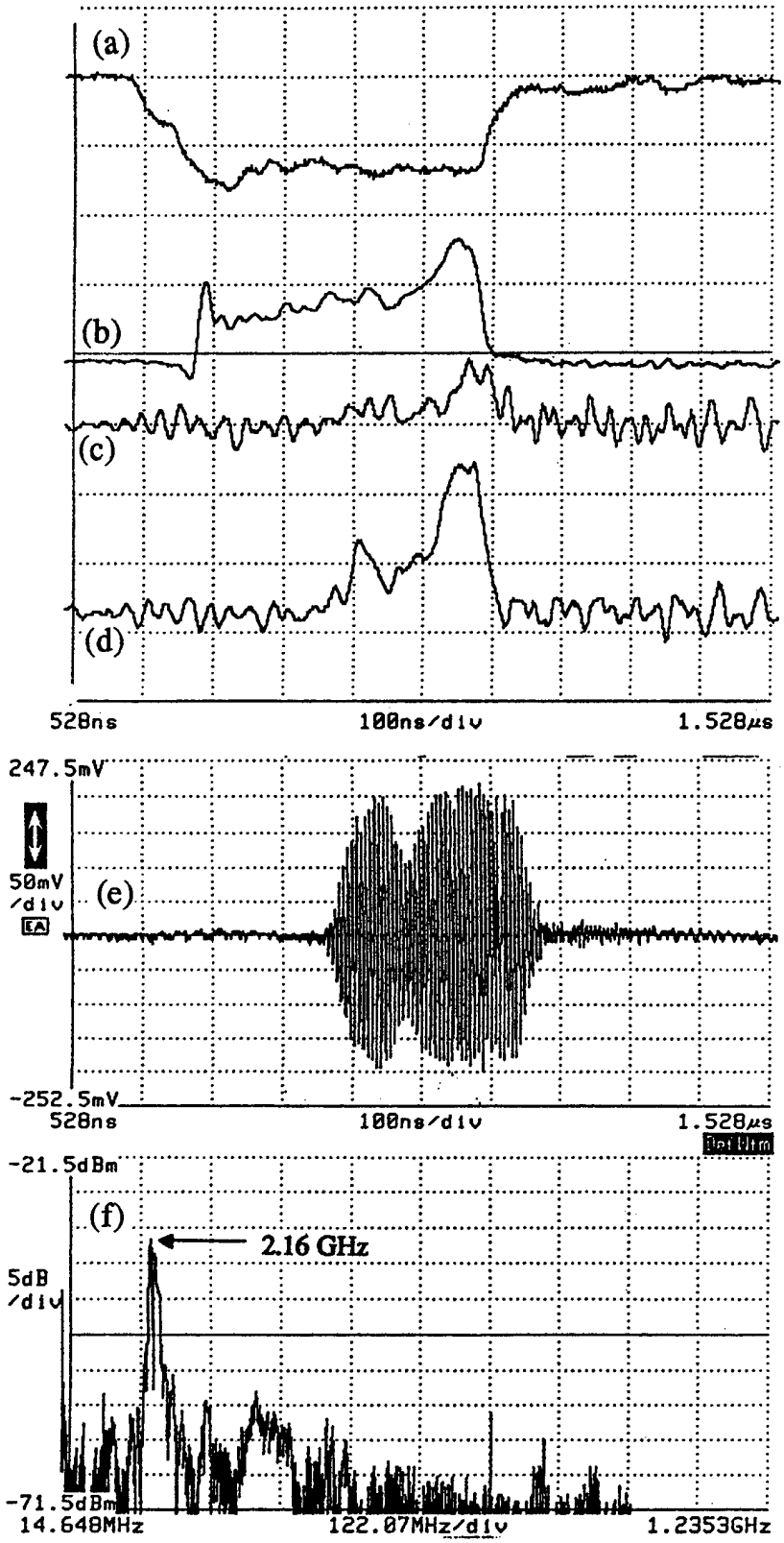

Fig. 4. Experimental data signals for the RCS large-orbit gyrotron cusp I with a cavity magnetic field of 1.5 kGauss, (a)–(e) time scale 100 ns/div. (a) MELBA voltage (620 kV/div). (b) RCS cavity entrance current (161 A/div). (c) Microwave detector signal for the TE_{01} polarized output (50 mV/div), peak power corresponds to 0.05 MW. (d) Microwave detector signal for the TE_{10} polarized output (50 mV/div), peak power corresponds to 11 MW. (e) Signal from single mixer with the local oscillator set at 2.0 GHz. (f) FFT of mixer signal showing an intermediate frequency of 0.16 GHz, giving a frequency of 2.16 GHz for the gyrotron-rf (frequency scale of 1.2207 MHz/div).

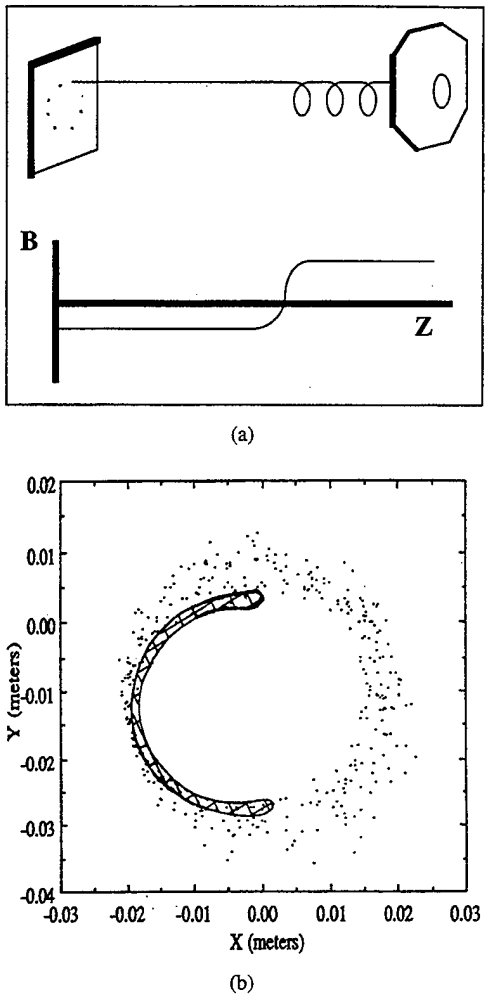

Fig. 5. (a) Model for glass plate alpha measurements, with axial B field profile. (b) Figure showing where experimental radiation darkening occurred on the glass plate (cross-hatched area) as compared with electron beam trajectory code results (individual points) for $\alpha = 1.0$.

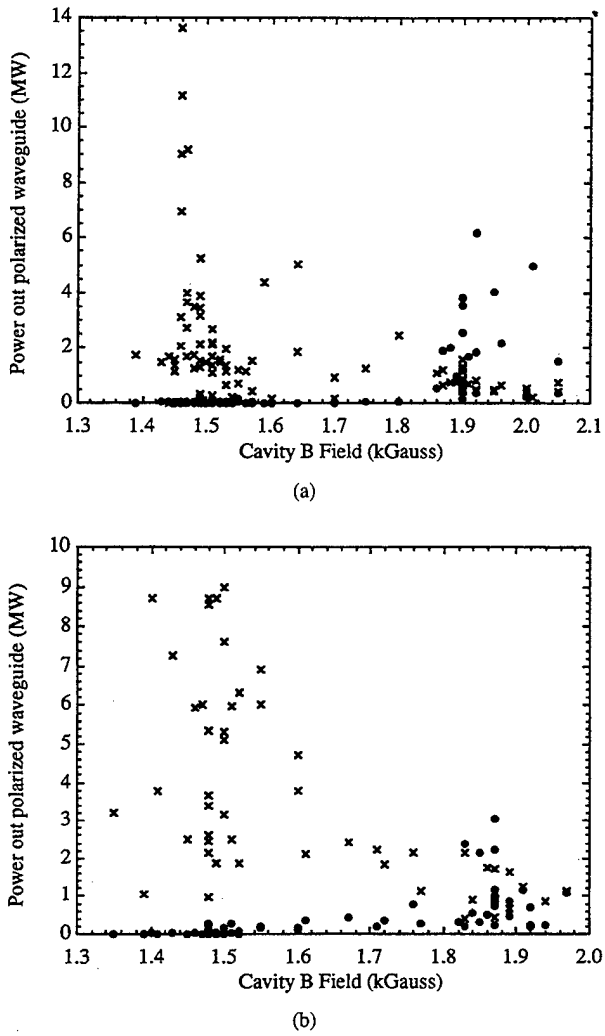

Fig. 6. Gyrotron microwave power radiated out of modified S-band waveguide as a function of cavity magnetic field for two different cusps. • = horizontal, TE_{01} polarization; × = vertical, TE_{10} polarization. (a) Cusp I. (b) Cusp II.

mode was the only mode present. As the interaction region magnetic field was raised, mode competition was visible. The TE_{102} mode (as opposed to the TE_{101} mentioned above) grew in magnitude to comparable levels to the fundamental mode, and the total microwave power in the vertically polarized mode (TE_{10}) dropped from 14 to 1 MW as the field increased to 1.9 kGauss. The TE_{102} mode was measured in heterodyne mixer measurements at 2.48 GHz. In contrast, the orthogonal TE_{01} mode grew from 50 kW to as high as 6 MW as the magnetic field was increased to 1.9 kGauss, as is shown in Fig. 6(a). As shown in cold testing, the cavity resonance occurred at 2.88 GHz for the TE_{011} mode; in experimental gyrotron emission measurements the resonance for this mode occurred at 2.87 GHz, in excellent agreement. In cusp II, for which the data is shown in Fig. 6(b), the fundamental mode power reached 9 MW at 1.5 kGauss and dropped to 2 MW at 1.9 kGauss. In the cusp II, the orthogonal TE_{011} mode reached 3 MW at higher fields (1.9 kGauss) and dropped off at both higher and lower fields. Both the TE_{111} mode at 3.5 GHz (for $B = \sim 1.9$ kGauss) and the TE_{201} mode at 3.99 GHz ($B = \sim 1.9$ kGauss) were also visible in some heterodyne mixer measurements, but they were on the order of 10–20 dB down from the TE_{101} and TE_{011} mode powers.

The polarization power ratios, which are defined here as the ratio of the RCS gyrotron's microwave power generated in the vertical mode (TE_{10}) to the power generated in the horizontal mode (TE_{01}) are demonstrated in Fig. 7(a) and (b) for the two cusps. In cusp I gyrotron, the fundamental mode dominated, as was shown by the power measurements in Fig. 6. The polarization power ratio achieved values as high as 300 at 1.48 kGauss, and the ratio dropped to as low as 0.05 $\{\mathrm{Pwr}(TE_{01})/\mathrm{Pwr}(TE_{10}) = 20\}$ for cusp I, (where the ratio of 1 implies equal power levels in the horizontal and vertical modes). Cusp II gyrotron reached higher polarization ratios with the fundamental TE_{10} mode dominating the TE_{01} mode by a factor as high as 1000. But, due to increased mode competition at higher magnetic fields, the polarization power ratio only dropped as low as 0.2 $\{\mathrm{Pwr}(TE_{01})/\mathrm{Pwr}(TE_{10}) = 5\}$ as the magnetic field was raised from 1.5 to 1.9 kGauss.

A measure of the device's operating efficiency, η, the electronic efficiency, is calculated as the ratio of the total

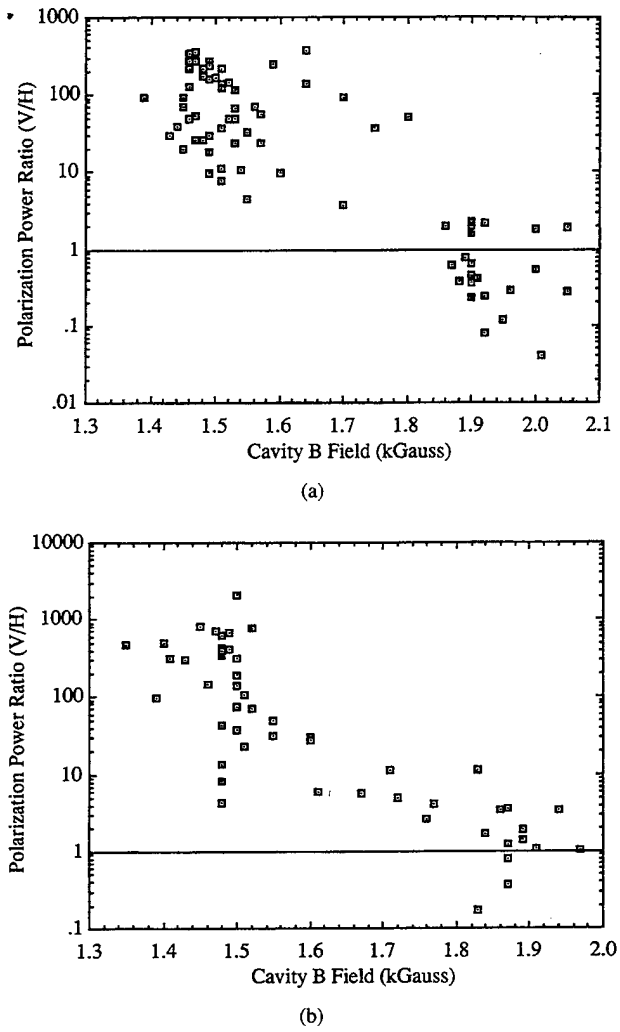

Fig. 7. Gyrotron microwave polarization power ratio for the two cusps as a function of cavity magnetic field. (a) Cusp I. (b) Cusp II.

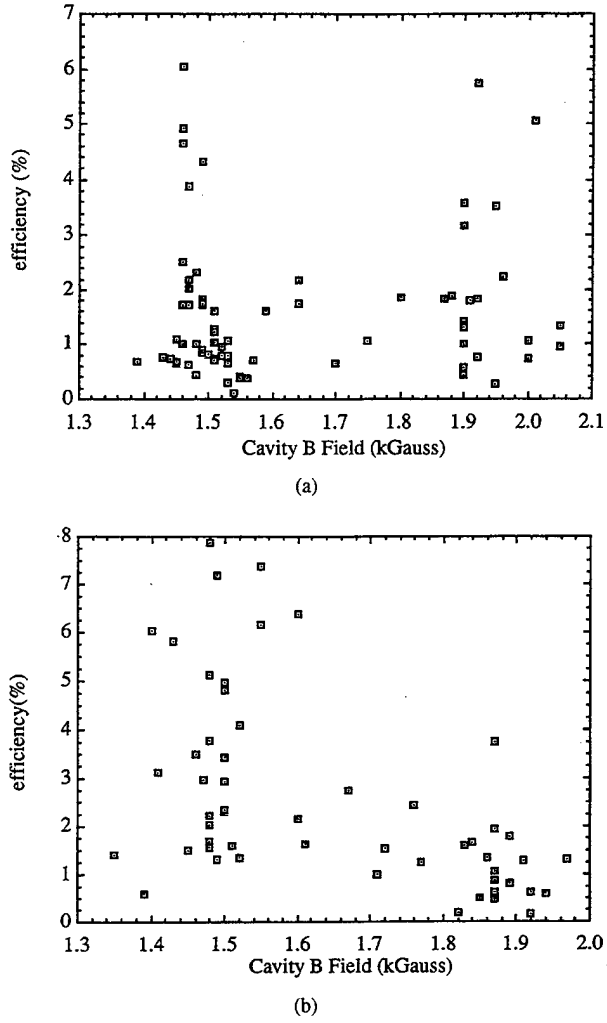

Fig. 8. Electronic efficiency of the RCS gyrotron as a function of magnetic field. (a) Cusp I. (b) Cusp II.

instantaneous microwave power (all modes) to beam power. Fig. 8(a) and (b) show the RCS gyrotron's electronic efficiency for both cusps. For cusp I, gyrotron efficiencies as high as 6% were measured at both low (1.48 kGauss) and high (1.9 kGauss) magnetic fields, with low efficiencies between them. Microwave production as shown in Fig. 6 was very small in the region between the two resonances. Fig. 8(b) shows the gyrotron's electronic efficiency for cusp II. In this case, the peak efficiency was 8%. Another measure of a gyrotron's efficiency is the perpendicular efficiency, $\eta_\perp$, which is due to the microwave power driven by the perpendicular energy of the beam, and it is calculated as follows [22]:

$$\eta_\perp = P_{\mu\text{wave}}/P_{\perp\text{beam}} = \eta(1 + 1/\alpha^2) \qquad (2)$$

Assuming the axis-encircling beam alpha is 1.0, the RCS gyrotron's peak $\eta_\perp$ yields approximately 16%.

The RCS gyrotron's experimental frequency spectra for the two cusps are shown in Fig. 9. Cusp I [Fig. 9(a)] gyrotron produced microwave radiation due to the following modes: $TE_{111}, TE_{011}, TE_{102}, TE_{101}$. The gyrotron experimental data from cusp II [Fig. 9(b)] showed similar results as cusp I. However, in a few Cusp II shots at higher B-fields (~1.9 kGauss), the TE_{201} mode also appeared. The heterodyne mixer data shown was confirmed by the modes measured in cold tests, as was discussed previously. The MAGIC 2D code simulations, which are discussed later, show some corroborations with the experimental (3-D) frequency measurements. The radiation from the fundamental TE_{101} mode was dominant at low B-fields (1.4–1.6 kGauss), and although other modes were present, their magnitudes were greater than 10 dB down (in most cases, 20 dB) from the fundamental mode. At higher B-fields, the TE_{011} mode was dominant, but the mode competition was significantly worse with other modes' power magnitudes on the order of the TE_{011} mode.

To examine at the effects of the cavity magnetic field on the polarization of microwave emission, electromagnetic particle-in-cell simulations were conducted utilizing the MAGIC Code [23]. Since the MAGIC Code was previously two dimensional, simulations were performed in X-Y coordinates, assuming the rectangular cavity was infinite in the Z direction; under this assumption k_z is zero. The cavity dimensions were set at 7.2 × 5.4 cm. Four beamlets were used to simulate an annular beam, and they were placed at a radius of approximately 1.8 cm. The beam voltage was set at 800 kV, with a beam alpha set

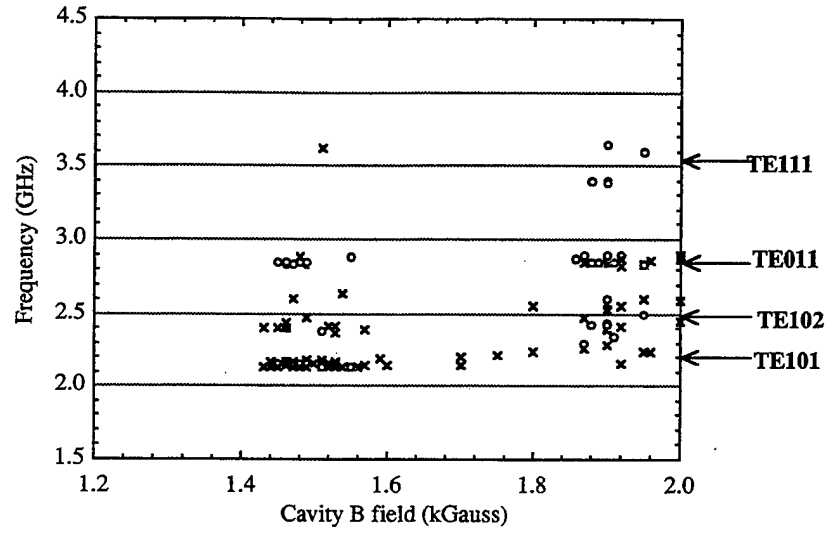

(a)

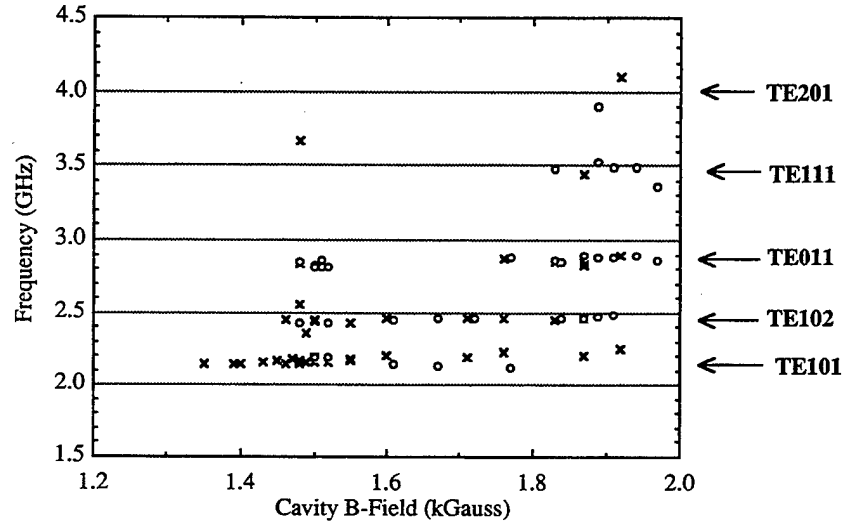

(b)

Fig. 9. Gyrotron microwave frequency data from the heterodyne mixer as a function of magnetic field. x = data taken from vertically polarized waveguide; o = data taken from horizontally polarized waveguide. Signals from the TE_{101} and TE_{011} modes were much stronger than other competing modes. (a) Cusp I. (b) Cusp II.

at 1.0 and current of 200 A for the four beamlets (total). The magnetic field was varied from 1.5–2.4 kGauss for different cases. The simulation was allowed to run for 30 ns. The time resolved E_x and E_y wave electric fields were found by the MAGIC code, as well as the peak amplitudes of the FFT electric fields. The voltage of the peak field amplitude due to the TE_{10} mode was compared with the peak field amplitude of the TE_{01} mode.

Results are shown in Fig. 10 of MAGIC code simulations performed on the rectangular cross section gyrotron. The model in Fig. 10(a) shows the parameters used in the simulations. As opposed to starting with an initial annular ring, the beam was prebunched by using the four beamlets. Within 10 ns the four beamlets appeared to bunch into two rotating bunches, and by the end of the simulation, at 30 ns, there appeared to be one larger bunch rotating in time with a group of individual particles spread around the axis. This apparently followed a phase bunching mechanism described for gyrotron interactions [5]–[7]. Fast Fourier transforms were observed of the electric fields in both the vertical and horizontal polarizations, with the magnitude of the peak amplitudes at the resonances for the two orthogonal modes (TE_{10}) and (TE_{01}). The corresponding power was then calculated using [24]

$$P = \sum_{m=1}^{\infty} \sum_{n=0}^{\infty} (Y_0)^*_{mn} |E_{mn}|^2 \frac{ab}{2\epsilon_n} \tag{3}$$

where

$$(Y_o)_{mn} = \frac{-H_x}{E_y} = \frac{k^2 - (m\pi/n)^2}{\omega \mu k_z} \tag{4}$$

$(Y_o)_{mn}$ are the TE_x wave admittances, a and b are the horizontal and vertical dimensions, respectively, ϵ is the permittivity, and k is the wave number. The ratio of the powers were then calculated, $P_{\text{vertical}}\{TE_{10}\}/P_{\text{horizontal}}\{TE_{01}\}$. These results are shown in Fig. 10(b). The resonances in the E-fields appeared at 2.16 and 2.85 GHz, respectively. Fig. 10(b) shows

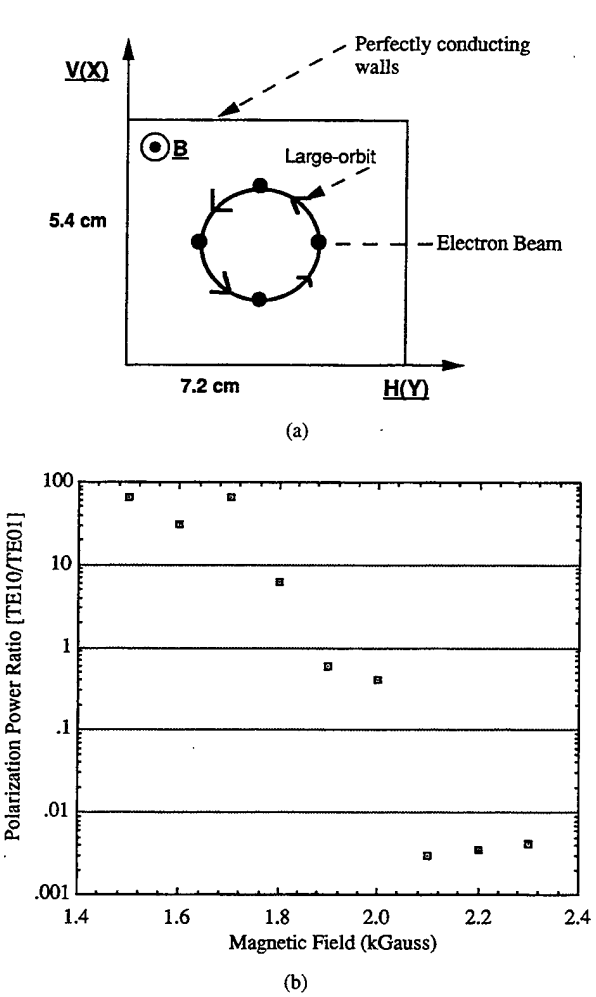

Fig. 10. (a) Model used for 2-D MAGIC code simulations of RCS gyrotron. (b) Microwave polarization power ratio as a function of B-field from MAGIC code simulations. The model assumes $k_z = 0$, beam alpha = 1.0, and beam current = 200 A.

that the fundamental TE_{10} mode is dominant at lower fields but rapidly transfers to the TE_{01} mode, which dominates at higher magnetic fields. Fig. 10(b) shows this change in polarization at 1.9 kGauss which agrees qualitatively with the experimental results. Due to assuming $k_z = 0$ in these simulations, the TE11 mode became dominant over either of the previous orthogonal modes at higher magnetic fields, on the order of 2.3 kGauss. The simulation predictions agree qualitatively with the experimental results but differ due to the restrictions placed on the simulation, i.e. two dimensionality.

IV. Conclusion

The experiments on the RCS gyrotron oscillator have demonstrated effective polarization control. Using the RCS gyrotron with MELBA, peak powers of 14 MW in one polarization (TE_{10}) and 6 MW in the cross-polarized mode (TE_{01}) were achieved. Electronic efficiencies for this device reached as high as 8% with transverse efficiency of 16%. Experimental results on beam diagnostics agree well with the single electron trajectory code, and computer simulations using MAGIC code are in qualitative agreement with results from microwave measurements. The polarization of high power megawatt microwaves can be controlled by varying only the cavity magnetic fields on an axis-encircling beam in a rectangular-cross-section gyrotron oscillator. Applications such as a rapid scanning radar, (where generating linearly polarized radiation in either of the TE_{10} or TE_{01} modes is necessary), could find the RCS gyrotron more useful than having to convert cylindrical waveguide output to the various linear modes.

Acknowledgment

The authors appreciate the experimental assistance from J. Luginsland, S. Kovaleski, A. Edson, and D. Love.

References

[1] V. L. Granatstein, *High-Power Microwave Sources*. Boston, MA: Artech House, 1987, ch. 5, p. 185.
[2] G. Benford and J. Swegle, *High Power Microwaves*. Boston, MA: Artech House, 1992.
[3] A. V. Gaponov-Grekhov and V. L. Granatstein, *Applications of High Power Microwaves*. Boston, MA: Artech House, 1994.
[4] W. Lawson and W. W. Destler, "The axially modulated, cusp-injected, large-orbit gyrotron amplifier," *IEEE Trans. Plasma Sci.*, vol. 22, p. 895, 1994.
[5] W. Lawson, P. E. Latham, J. P. Calame, J. Cheng, B. Hogan, G. S. Nusinovich, V. L. Granatstein, and M. Reiser, "High power operation of first and second harmonic gyrotwystrons," *J. Appl. Phys.*, vol. 78, p. 550, 1995.
[6] W. W. Destler, E. Chojnacki, R. F. Hoeberling, W. Lawson, A Singh, and C. D. Strifler, "High-power microwave generation from large-orbit devices," *IEEE Trans. Plasma Sci.*, vol. 16, p. 71, 1988.
[7] W. Lawson, "Generation of microwave radiation from annular, rotating electron beams in various waveguide geometries," Ph.D dissertation, Univ. Maryland, College Park, 1985.
[8] S. H. Gold, A. W. Fliflet, W. M. Manheimer, R. B. McCowan, R. C. Lee, V. L. Granatstein, D. L. Hardesty, A. K. Kinkead, and M. Sucy, "High peak power Ka-band gyrotron oscillator experiments with slotted and unslotted cavities," *IEEE Trans. Plasma Sci.*, vol. 16, pp. 142–148, Apr. 1988.
[9] W. M. Black, S. H. Gold, A. W. Fliflet, D. A. Kirkpatrick, W. M. Manheimer, R. C. Lee, V. L. Granatstein, D. L. Hardesty, A. K. Kinkead, and M. Sucy, "Megavolt, multi-kiloamp Ka-band gyrotron oscillator experiment," *Phys. Fluids B*, vol. 2, pp. 193–198, Jan. 1990.
[10] J. Benford, "Applications of high power microwaves to modification and measurement of the atmosphere," *SPIE OE'LASE Conf.*, Los Angeles, CA, Jan. 1993.
[11] R. M. Gilgenbach, M. E. Read, K. E. Hackett, R. Lucey, B. Hui, V. L. Granatstein, K. R. Chu, A. C. England, C. M. Loring, O. C. Eldridge, A. C. Howe, A. G. Kulchar, E. Lazarus, M. Murakami, and J. B. Wilgen, "Heating at the electron cyclotron frequency in ISX-B tokamak," *Phys. Rev. Lett.*, vol. 44, pp. 647–650, 1980.
[12] W. Lawson and P. E. Latham, "The design of a small-orbit/large-orbit gyroklystron experiment," *J. Appl. Phys.*, vol. 61, p. 519, 1987.
[13] W. W. Destler, K. Irwin, W. Lawson, J. Rodgers, Z. Segalov, E. P. Scannell, and S. T. Spang, "Intense beam fundamental mode large-orbit gyrotron studies," *J. Appl. Phys.*, vol. 66, p. 4089, 1989.
[14] Y. Y. Lau and L. R. Barnett, "Theory of a low magnetic field gyrotron-gyromagnetron," *Int. J. Inf. Millim. Waves*, vol. 3, p. 619, 1982.
[15] D. J. Radack, K. Ramaswamy, W. W. Destler, and J. Rodgers, "A fundamental mode, high-power, large-orbit gyrotron using a rectangular interaction region," *J. Appl. Phys.*, vol. 73, pp. 8139–8145, Feb. 1993.
[16] Y. Y. Lau and L. R. Barnett, "A note on gyrotron traveling-wave amplifiers using rectangular waveguides," *IEEE Trans. Electron Devices*, vol. ED-30, p. 908, 1983.
[17] Y. Y. Lau, L. R. Barnett, and J. M. Baird, "An active circulator-gyrotron traveling-wave amplifier," *IEEE Trans. Electron Devices*, vol. ED-31, pp. 337–347, Mar. 1984.
[18] R. M. Gilgenbach, J. M. Hochman, R. Jaynes, M. T. Walter, J. I. Rintamaki, J. S. Lash, Y. Y. Lau, J. W. Luginsland, and T. A. Spencer, "High power microwave emission and diagnostics of microsecond

electron beams," *Proc. Infrared Millimeter Waves Conf.*, Orlando, FL, Dec. 1995.
[19] J. M. Hochman, R. M. Gilgenbach, R. L. Jaynes, J. I. Rintamaki, Y. Y. Lau, J. W. Luginsland, J. S. Lash, and T. A. Spencer, "Rectangular cross-section high power gyrotron," *Proc. SPIE Conf. Intense Microwave Pulses IV*, vol. 2843, p. 38, 1996.
[20] J. J. Choi, R. M. Gilgenbach, T. A. Spencer, P. R. Menge, and C. H. Ching, "Measurement of long-pulse relativistic electron beam perpendicular-to-parallel velocity ratio by Cerenkov emission and radiation darkening on a glass plate," *Rev. Sci. Instrum.*, vol. 63, no. 2, pp. 1671–1675, Feb. 1992.
[21] J. C. Slater, *Microwave Electronics*. New York: Van Nostrand, 1956.
[22] M. Walter, "Effects of tapering on high current, long pulse gyrotron backward wave oscillator experiments," Ph.D. dissertation, Univ. Michigan, Ann Arobr, 1995.
[23] B. Goplen, L. Ludeking, D. Smithe, and G. Warren, *MAGIC User's Manual*, Mission Research Corp. Rep. MRC/WDC-R-282, 1991.
[24] R. F. Harrington, *Time-Harmonic Electromagnetic Fields*. New York: McGraw-Hill, 1961, ch. 4.

Jonathan M. Hochman (S'97), for a photograph and biography, see this issue, p. 289.

Ronald M. Gilgenbach (S'73–M'74–SM'92), for a photograph and biography, see this issue, p. 288.

Reginald L. Jaynes, for a biography, see this issue, p. 289.

Joshua I. Rintamaki, for a biography, see this issue, p. 289.

Y. Y. Lau, for a photograph and biography, see this issue, p. 234.

William E. Cohen, for a biography, see this issue, p. 289.

Chris W. Peters, for a biography, see this issue, p. 289.

Thomas A. Spencer (M'94–SM'95), for a biography, see this issue, p. 289.